Technology Collaboration Programme
by IEA

Technology Collaboration Programme on Heat Pumping Technologies (HPT TCP)


# Annex 51

# Acoustic Signatures of Heat Pumps

## Final Report – Part 10

## Report on Task 4
## Analysis of the Effect of Operating Conditions of Heat Pumps on Acoustic Behaviour

Editors:
Thomas Gindre, Thore Oltersdorf (Fraunhofer ISE),
Christian Vering (RWTH Aachen), Johann Emhofer,
Christoph Reichl (AIT), Kamalathasan Arumugam (DTI)

June 2021

Report no. HPT-AN51-10

**Published by**

Heat Pump Centre
c/o RISE – Research Institutes of Sweden
Box 857, SE-501 15 Borås
Sweden
Phone +46 10 16 53 42

**Website**

https://heatpumpingtechnologies.org

**Legal Notice**

Neither the Heat Pump Centre nor any person acting on its behalf:
(a) makes any warranty or representation, express or implied, with respect to the information contained in this report; or
(b) assumes liabilities with respect to the use of, or damages, resulting from, the use of this information.
Reference herein to any specific commercial product, process, or service by trade name, trademark, manufacturer, or otherwise, does not necessarily constitute or imply its endorsement recommendation or favoring.
The views and opinions of authors expressed herein do not necessarily state or reflect those of the Heat Pump Centre, or any of its employees. The information herein is presented in the authors' own words.



**Production**

Heat Pump Centre, Borås, Sweden

**ISBN 978-91-89561-66-3**
**Report No. HPT-AN51-10**

# Preface

This project was carried out within the Technology Collaboration Programme on Heat Pumping Technologies (HPT TCP), which is a Technology Collaboration Programme within the International Energy Agency, IEA.

### The IEA

The IEA was established in 1974 within the framework of the Organization for Economic Cooperation and Development (OECD) to implement an International Energy Programme. A basic aim of the IEA is to foster cooperation among the IEA participating countries to increase energy security through energy conservation, development of alternative energy sources, new energy technology and research and development (R&D). This is achieved, in part, through a programme of energy technology and R&D collaboration, currently within the framework of nearly 40 Technology Collaboration Programmes.

### The Technology Collaboration Programme on Heat Pumping Technologies (HPT TCP)

The Technology Collaboration Programme on Heat Pumping Technologies (HPT TCP) forms the legal basis for the implementing agreement for a programme of research, development, demonstration, and promotion of heat pumping technologies. Signatories of the TCP are either governments or organizations designated by their respective governments to conduct programmes in the field of energy conservation.

Under the TCP, collaborative tasks, or “Annexes”, in the field of heat pumps are undertaken. These tasks are conducted on a cost-sharing and/or task-sharing basis by the participating countries. An Annex is in general coordinated by one country which acts as the Operating Agent (manager). Annexes have specific topics and work plans and operate for a specified period, usually several years. The objectives vary from information exchange to the development and implementation of technology. This report presents the results of one Annex.

The Programme is governed by an Executive Committee, which monitors existing projects and identifies new areas where collaborative effort may be beneficial.

### Disclaimer

The HPT TCP is part of a network of autonomous collaborative partnerships focused on a wide range of energy technologies known as Technology Collaboration Programmes or TCPs. The TCPs are organized under the auspices of the International Energy Agency (IEA), but the TCPs are functionally and legally autonomous. Views, findings and publications of the HPT TCP do not necessarily represent the views or policies of the IEA Secretariat or its individual member countries.

### The Heat Pump Centre

A central role within the HPT TCP is played by the Heat Pump Centre (HPC).

Consistent with the overall objective of the HPT TCP, the HPC seeks to accelerate the implementation of heat pump technologies and thereby optimize the use of energy resources for the benefit of the environment. This is achieved by offering a worldwide information service to support all those who can play a part in the implementation of heat pumping technology including researchers, engineers, manufacturers, installers, equipment users, and energy policy makers in utilities, government offices and other organizations. Activities of the HPC include the production of a Magazine with an additional newsletter 3 times per year, the HPT TCP webpage, the organization of workshops, an inquiry service and a promotion programme. The HPC also publishes selected results from other Annexes, and this publication is one result of this activity.

For further information about the Technology Collaboration Programme on Heat Pumping Technologies (HPT TCP) and for inquiries on heat pump issues in general contact the Heat Pump Centre at the following address:

Heat Pump Centre
c/o RISE - Research Institutes of Sweden
Box 857, SE-501 15 BORÅS, Sweden
Phone: +46 10 516 53 42
Website: https://heatpumpingtechnologies.org

Acoustic Signatures of Heat Pumps
IEA HPT Annex 51

# Report on Task 4: Analysis of the Effect of Operating Conditions of Heat Pumps on Acoustic Behaviour

*System modelling, including acoustics for control, and studies on time dependent behaviour as well as influence of external conditions.*

Contributors: Thomas Gindre, Thore Oltersdorf (Fraunhofer ISE), Christian Vering (RWTH Aachen), Johann Emhofer, Christoph Reichl (AIT), Kamalathasan Arumugam (DTI)

| | |
|---|---|
| Date: June 2021 | Final Version, Review: 04 |

# Contents

# Introduction

The world's climate is changing faster than ever and the European public is more and more informed and aware of it. The anthropogenic climate change due to the wasteful usage of fossil fuels is one of the central challenges in the 21st century. In order to assume responsibility for future generations it is important to meet this challenge with appropriate measures and urgency.

Energy used for heating and cooling together account for almost 50 percent of the EU's total primary energy demand [1]. Hence, moving towards efficient and environment-friendly heating systems can significantly reduce primary energy consumption. In this context, heat pumps have been identified as a key technology for heating and cooling. They should get to play an increasingly important role in the decarbonization of the heating sector, for they feature a high energy efficiency and most operate on electricity to extract heat from their environment. By operating them with green electricity, almost zero $C0_2$ emissions can be reached [2].

However, heat pumps are complex devices featuring various noisy components. When used in large numbers in urban areas, heat pumps emit a considerable amount of noise. Given the technological advancements of the past decades to optimize the energetic aspects, the inconveniences caused by their noise emissions are to represent the main obstacle to their market penetration.
In the Annex51 Task 1 report, the national laws and regulations regarding noise protection of some European member states are summarised, including regulations which specifically address noise emissions from heat pumps.
In the Annex51 Task 3 report, those noises are identified at the component and units levels, and the corresponding noise control techniques are discussed.

Even though other types without fans exist, such as ground-source heat pumps, air-to-water (A/W) heat pumps have become increasingly popular in recent years due to their advantages such as small space requirements, comparatively low purchase costs, simple installation, etc. and are among the most sold heat pump systems for heating or cooling residential buildings in Europe. In addition to the annoying noise of the compressor, the high air volume flow required by the heat pump often causes annoying noise from the fan and evaporator. Especially during the transitional season, additional noise is generated due to icing of the evaporator. All these annoying noises often trigger neighbourhood conflicts with health, psychological and financial consequences, and can thus become a competitive disadvantage for the future of this technology and hinder its widespread use, especially in residential areas.

Furthermore, the nature and intensity of those emitted noises can strongly depend on the heat pump operating conditions. In this report, the state of knowledge over the acoustical impact of operating conditions of heat pumps is investigated. Even though other types without fans exist, such as ground-source heat pumps, this is primarily centered on air-to-water (A/W) heat pumps, as they represent the most common type and feature all the most significant noise sources as well as the least flexibility with regard to the location of installation.

To this purpose, the focus is first laid on tools allowing for a modelling of heat pump acoustic emissions as a function of its operating state.

The noises resulting of transient operations are then examined, beginning with a description of the physical processes likely to produce the most obvious or bothersome noises, before describing them

by order of time scale. When possible, recommendations as to how to reduce the influence of those acoustic emissions are discussed.

Finally, the dependency on the type of heat source and the temperature and load levels are examined.

## Acoustic modelling of heat pumps

As shown in the Annex51 Task3 report (cf. Figure 1), the acoustic behaviour of heat pumps features a high complexity, with structure-borne, fluid-borne and air-borne noise generation plus their mutual interactions. All those aspects are strongly dependent on the investigated appliance, its location, its operating point and its control strategy (i.e. the program using sensor data as input to control the various motors and actuators of the device in order to ensure stable operation at the desired capacity).

Even if several methods exist to accurately describe sound propagation, they prove to be very computationally intensive. Their potential use to describe or control the sound propagation from transient thermodynamic events within the complexity of heat pumps is therefore limited.

To close this gap and efficiently assess the noise propagation in conjunction with transient thermodynamic operations, the Austrian Institute of Technology has instigated the development of a library in Modelica: the Sound Source Extension library [2], which enables a 1D model of the sound propagation, relying on experimental measurements and coupled with an energetic model. This tool is presented in the following section.

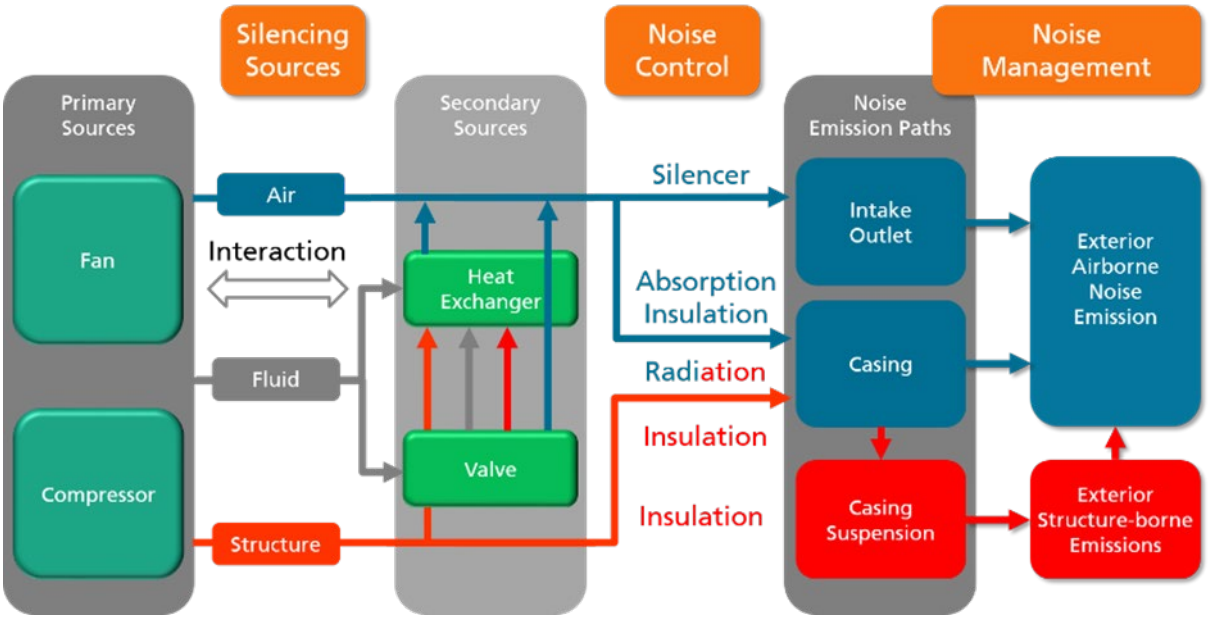


**Figure 1: Block diagram showing the heat pump primary and secondary noise sources and main airborne and structure-borne transfer paths to the exterior [3].**

## Modeling and simulation of coupled thermodynamics and acoustics – SSElib

As extension of the open source Modelica software (or the proprietary Dymola), the Sound Source Extension library ("SSElib") uses a low dimension acoustical model to assess the radiated airborne sound depending on the thermodynamic operating conditions of the system and its noise reduction measures.

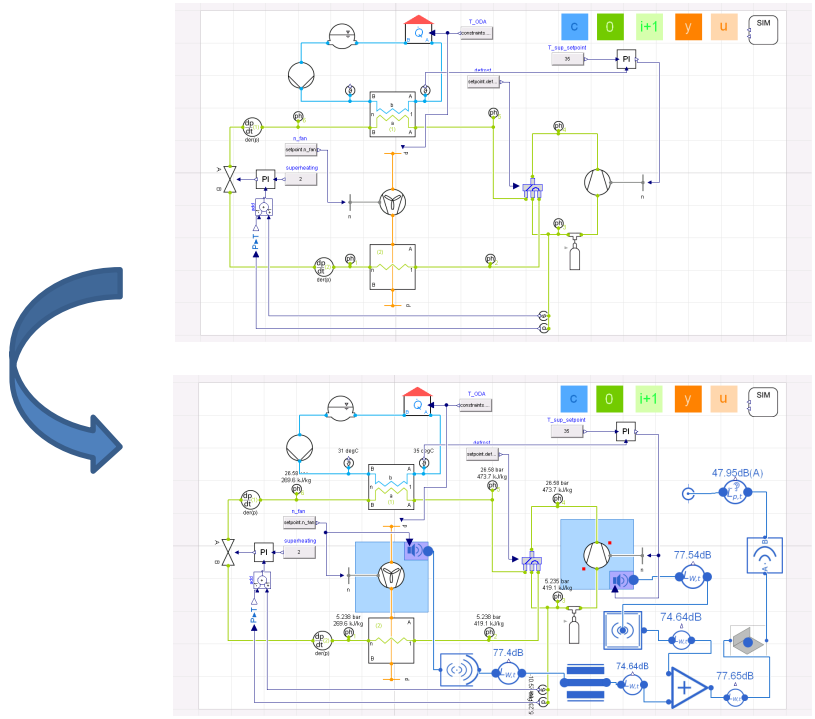


**Figure 2: A thermodynamic heat pump model gets extended with components out of the SSE library. Extract from [2]**

The SSElib is well suited to acoustically model not only stationary but also transient heat pump operations, as it is frequency based (for now per octave bands) with a spectrum which can in turn depend on an operational parameter of some components, typically the rotational speed of a motor or compressor:

**Assumptions:**

- All sound sources are independent point sources.
- The sound fields considered in the SSElib are assumed to be diffuse and incoherent in all frequencies.
- There are restrictions on the noise source volume, to fulfill the conditions required for diffuse and reverberant approximation.

**Advantages:**

- Easy coupling with existing Modelica models (in particular thermodynamic models, see next chapter on Energetic-Acoustic Optimal Operation)
- Quick computation of the sound pressure and power level for each octave band (Figure 3)
- Operating state as input parameter (e.g. rpm of a compressor)
- Provided with a library of standard components and sensors.

- Possibility to interpolate experimental SWL data as polynomial functions of some operating parameter (see also Figure 4 and Acoustic Coupling in the next chapter on Energetic-Acoustic Optimal Operation)

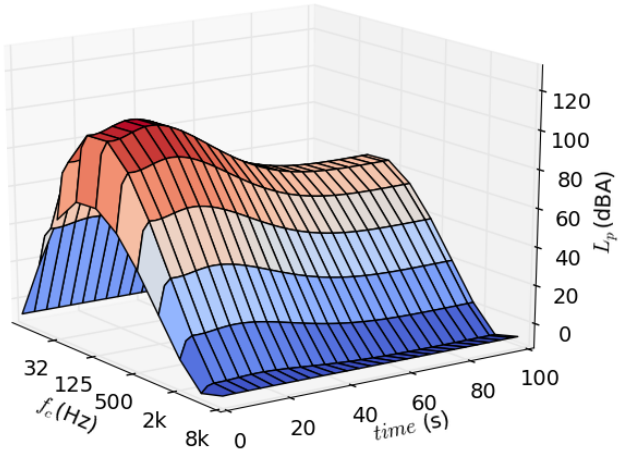


**Figure 3: Transient behaviour of the heat pump in the one-octave band of centre frequency $f_c$. Extract from [2]**

**Downsides:**

- The library only computes radial symmetry and 1D sound propagation, it can't take complex system geometry into account.
- Doesn't directly account for the propagation of vibrations through the structure.
- Low dimensional: only for approximations of the radiated airborne sound.

→ The SSElib makes the link between the SWL of the separate components of a system and its total radiated power. Even if to be considered only as approximation, the results allow not only for an optimization of the passive sound attenuation measures but also that of the heat pump control strategy.

For the latter, this acoustic model needs to be coupled with an energetic model of the heat pump. The next section presents the work of RWTH Aachen towards a combined energetic and acoustic optimization of heat pump operation.

## Modelling and simulation of an energetic-acoustic optimal operation (EAO)

Ideally, the control strategy of a heat pump can take external conditions and heat demand into account to enable both energy efficient operation and low noise emissions. As it turns out, this is a complex task, as energetic and acoustic aspects tend to constitute a conflict of objectives.

Simulation models are suitable for testing of new control concepts, since they allow easy modification of the systems in comparison to test bench trials. Investigations can be carried out efficiently, which decreases both development time and costs. Depending on the level of detail, simulations can be faster calculated than real time, so that systems can be analysed in very long time intervals that are not economically observable in reality.

The combined optimization of control strategy therefore requires the coupling of an energetic and an acoustic model. Such work got conducted at the RWTH Aachen and is presented here, first with regard to the energetic model alone, then to the coupling with acoustics, and finally to the simultaneous energetic and acoustic evaluation and optimization.

## Energetic modelling of system components

Heat pumps consist of four main components:

- Compressor
- Condenser
- Expansion valve
- Evaporator

These components are modelled in Modelica using Dymola and was first published in [4]. The models are open-source available at GitHub[1]. Other libraries providing heat pump models are the freely available ThermoCycle library[2], and the commercially available TIL library[3], which allows for realizing the circuit with a four-way valve for circuit reversal.

### *Compressor*

The compressor of a heat pump has the task to compress refrigerant by supplying external work to an increased pressure and thus also temperature level [2, 3]. A semi-empirical efficiency-based modelling approach is chosen as it describes a good compromise of accuracy and simulation speed.

For this purpose, the compression process is completely described with three efficiencies. Efficiencies include the isentropic efficiency as functions of enthalpies $h_i$:

$$\eta_{is} = \frac{h_{2,\mathrm{is}} - h_1}{h_2 - h_1}$$

The volumetric efficiency as ratio of mass flow rates $\dot{m}_i$

$$\lambda_h = \frac{\dot{m}}{\dot{m}_{\mathrm{ideal}}}$$

And the effective, mechanical efficiency as ratio of compressed power $P_{\mathrm{Fluid}}$ divided by electrical power at the inverter $P_{\mathrm{inv}}$:

$$\eta = \frac{P_{\mathrm{Fluid}}}{P_{\mathrm{Comp}}}$$

Using measurement data correlations, the efficiencies are determined as a function of the pressure ratio $\Pi$, the compressors' rotational speed $n$ and the compressor inlet temperature $T_{\mathrm{in}}$. The model is very fast and stable due to the simple description. The modelling accuracy depends on the quality of the measured data correlation and its accuracy is considered sufficient for the current purpose.

### *Heat exchangers*

Both condenser and evaporator are modelled applying $\epsilon - NTU$ method. The transferred heat flow $\dot{Q}$ is determined via an efficiency factor from the maximum transferred heat flow $\dot{Q}_{\mathrm{max}}$ according to the following formula:

$$\epsilon = \frac{\dot{Q}}{\dot{Q}_{\mathrm{max}}}$$

[1] https://github.com/RWTH-EBC/AixLib
[2] http://www.thermocycle.net/
[3] https://www.tlk-thermo.com/index.php/de/til-suite

The efficiency factor can be calculated depending on the flow in the heat exchanger (parallel flow, counter flow, cross flow) using the dimensionless ratios $R$ and $NTU$ can be approximated. The ratio $R$ describes the dimensionless ratio of the heat capacity currents and assumes values between 0 and 1. Accordingly, for $R$:

$$0 \leq R = \frac{(\dot{m} * c_p)_1}{(\dot{m} * c_p)_2} \leq 1$$

The Number-of-Transfer-Units ($NTU$) determines the ratio of the constructive number $kA$ and the heat capacity current according to:

$$0 \leq NTU_1 = \frac{kA}{(\dot{m} * c_p)_1} \leq \infty$$

The $\epsilon - NTU$ method is regarded as a highly simplified method for modelling heat exchangers, but it can achieve high accuracy for static operating points. There is no division of the heat capacity flow by physical state, so only one heat transfer correlation per medium is considered. This is a disadvantage in modelling the phase change of refrigerants in heat pumps. In addition, liquid phase of the refrigerant has a higher heat transfer coefficient than the vapour phase. This leads to an underestimation of the heat transfer coefficient in case of an increased level of subcooling in the condenser.

For the evaporator, a heat transfer correlation for flat plates with isothermal surface and laminar boundary layer was implemented in the form:

$$Nu = 0.664\, Re^{1/2} Pr^{1/3}, for\ Re < 2 * 10^5$$

This considers the dependency of fan speed on heat transfer coefficient of air due to different air flow velocities. The other heat transfer coefficients are simplified and assumed to be constant.

Since the mass of the heat exchanger is not modelled with this method, the thermally inert behaviour cannot be reproduced. Via PT1 elements, however, the transferred heat output can be delayed with a dead time, so that the inertial behaviour can be approximated.

The advantages of the $\epsilon - NTU$ method are the high simulation speed and a robust modelling approach. Alternative approaches to the detailed physical description of heat transfer, such as the Moving Boundary Approach or the Finite-Volume Method, are disregarded here because of numerical instabilities and the high simulation times.

### *Expansion Valve*

The model of the expansion valve is based on Bernoulli's energy equation for incompressible fluids under the assumption of a constant enthalpy change of state. This assumption is justified because the change in specific enthalpy via the expansion valve is comparatively small. The mass flow rate flowing through is thus calculated as:

$$\dot{m} = C * z * A_{\text{total}} \sqrt{2\rho_3 (p_3 - p_4)}$$

$A_{\text{total}}$ is the cross-sectional area at maximum valve opening. The relative opening of the valve is described by the variable $z$. The flow coefficient $C$ takes into account any refrigerant behaviour that

deviates from Bernoulli's assumptions. For the application, the assumptions of a single-phase, incompressible and frictionless flow must be compensated. The flow coefficient is determined by semi-empirical data correlations and is valid for low pressure drops $\Pi$.

### *Fan*

The fan model was taken from AixLib [1, 7]. Applying Bernoulli equation and a simplified propeller, the system characteristic curve of a fan can be determined. According to this, the pressure increase of fan power correlates to quadratic volume flow:

$$p \propto \dot{V}^2$$

Finally, electric energy consumption is calculated using the equation:

$$W_{el} = \frac{\dot{V}\Delta p}{\eta_{\mathrm{Fan}}}$$

The combination of the both equations results in a cubic dependence of the electrical consumption on the rotational speed.

### *Parametrization*

The models have a number of parameters that have to be defined in order to map the behaviour of a specific heat pump. The parameters include heat transfer surfaces, the heat transfer coefficients, the displacement of the compressor and the cross-sectional area of the expansion valve. For parameterisation, a data record of an 8 kW air-to-water heat pump is available. This is adapted from records containing the $COP$ and the amount of heat emitted when the outside temperature varies, the compressor speed and the flow temperature. A mass flow of 0.1 kg/s and a water-side temperature difference of ΔT = 10 K are assumed. The parameters are varied manually until the behaviour can be represented in an acceptable way at the requested operating points. The quality of the parametrization depends on the size and precision of the dataset.

For subsequent work, the automated parameterization of the simulation model using a statistical optimizer, such as a genetic algorithm, is recommended for the successive individual validation of the component models. In this way, for example, individual Nusselt correlations can be determined for exact modelling of heat transfer. For further investigations, however, an exactly parameterized model is not essential, since changes to the simulation model are always compared with a reference state, so that absolute values are not used. The simulation model is thus classified as sufficiently accurate.

## Acoustic Coupling

At the example of an A/W heat pump with inverter-controlled scroll compressor, the acoustic signatures of the components are recorded separately from each other, without making any structural changes to the system. To measure the acoustic signature of the compressor, it is operated at various speeds, while the pump and the fan are operated at the lowest possible speed, to avoid measuring influences of further components. Measuring the acoustic signature of the fan, its speed is varied with both the compressor and pump switched off.

In order to couple the measurement data with the energetic simulation model, the acoustic signature is correlated with the speed of the respective component. The Sound Source Extension Library "SSElib" of the AIT is used to connect to the energetic model. The library has components to determine the sound propagation in the air, the effects of silencers and the installation location. In addition, several sound sources can be superimposed (cf. previous section).

The energetic models are thus extended by an acoustic interface. For this purpose, a correlation between acoustic measurement data and the speed of the component is stored. Since the SSElib was first implemented for octave bands, the models used are extended to fit with measurement data in third octave bands.

When transferring acoustic data to the acoustic interface, there is a conflict of objectives between the accuracy of the measured data and the simulation speed. The integration of the measured values as a 3D table with double interpolation for the determination of intermediate values is accurate but also computationally intensive. Therefore, Emhofer et al. of the AIT propose the introduction of a multivariable polynomial of the form:

$$L_p(x,y) = \sum_{i=0}^{n}\sum_{j=0}^{m} p_{i,j} x^i y^j$$

Herein $x$ denotes the speed of the component and $y$ the index of the one-third octave band. The frequency bands are split logarithmically, which makes regression difficult. Therefore, the one-third octave bands are numbered in ascending order and the index is used as an input variable for regression. For the polynomial function, coefficients are calculated using a polynomial adjustment calculation.

Assessing the regression quality thanks to the root mean square deviation ($RMSE$), it can be observed that some components are reproduced quite poorly, especially if featuring outliers in the measured values.

As increasing the polynomial degree $n$ doesn't lead to an improvement of the regression quality, an alternative approach is implemented, in which a polynomial is used for each one-third octave band depending on the speed (Figure 4). Thus, the sound pressure level is composed according to the following polynomial function:

$$L_p(x) = \sum_{i=0}^{5} p_i x^i \;\; \forall\, y \;\in [1,..,29]$$

Since a polynomial function is now determined for each one-third octave band, the measurement data can be mapped with increased accuracy. This leads to a drastic improvement of the accuracy,

with RMSE values comparatively several times smaller. The improvement of the regression quality is achieved by increasing the number of polynomial coefficients.

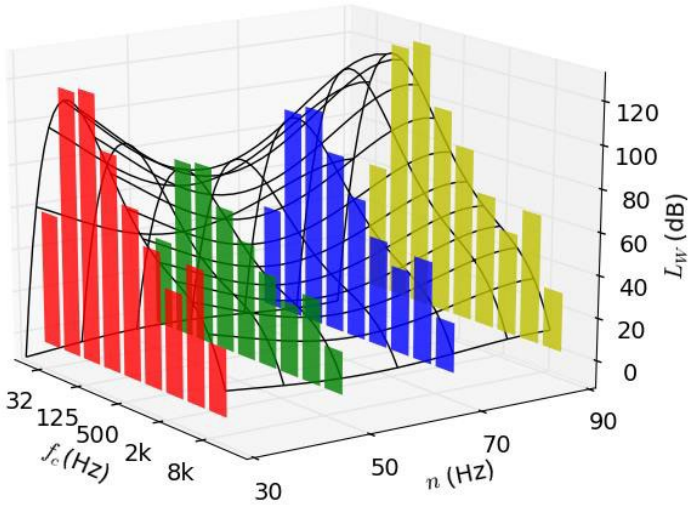


**Figure 4: polynomial SWL interpolation per octave band of center frequency $f_c$, as function of the compressor rotational speed $n$, based on 4 experimental datasets. [2]**

## Simultaneous energetic and acoustic evaluation of heat pumps

The aim is to operate the heat pump in an energy-acoustic optimum mode specified by the user. Therefore, acoustic emissions of the heat pump are evaluated simultaneously with the energy efficiency of the system. This is realized with the help of a model-free adaptive optimization method, the extremum seeking control (ESC), by introducing the conflict of objectives between energy efficiency and acoustic emission, then specifying a target function, and finally testing the ESC on a realistic operating sequence and evaluating the results.

### *Conflict of optimization between energy efficiency and acoustic emissions*

The noise emissions of heat pumps lead to acoustic discomfort for the user, neighbours and the environment. However, the customer's requirements for energy-efficient operation and at the same time quiet operation are in opposite directions, as illustrated by the following study.

In a simulation, the fan speed is varied at constant heat supply and constant ambient temperature (A7W50). Figure 5 shows the resulting curves of the coefficient of performance $COP$ and the sound pressure level $L_\mathrm{p}$ for different fan speeds. For this purpose, the fan speed is normalized as follows:

$$n_{Fan}^{*} = \frac{n_{Fan}}{n_{Fan,n}} \in [0,1]$$

where $n_{Fan,n}$ is the nominal fan speed. The correlation between condenser, evaporator and compressor solves an energy balance for the entire heat pump. The following applies:

$$\dot{Q}_\mathrm{Cond} = \dot{Q}_\mathrm{Evap} + P_\mathrm{Comp}$$

A change in fan speed $n$ results in a change of air mass flow and therefore, in a change of transferred heat at the evaporator. To achieve the constant heat dissipation at the condenser, the compressor capacity must be adjusted accordingly. For this purpose, the compressor speed is regulated. Obviously, an increase of fan speed leads to a decrease in compressor speed.

If the fan output is neglected, the $COP$ of the heat pump is:

$$COP = \frac{\dot{Q}_\mathrm{Cond}}{P_\mathrm{Comp}}$$

An increase in the fan speed always leads to an increase in the $COP$ (compare Figure 5 blue, dashed).

However, there is in fact a limit value above which the increase in electrical power of the fan is larger than the resulting decrease in electrical power at the compressor. This point represents the energetic optimum of the system. Thus, we define a system $COP$, where the fan power is considered in overall energy consumption:

$$COP = \frac{\dot{Q}_\mathrm{Cond}}{P_\mathrm{Comp} + P_\mathrm{Fan}}$$

Hence, Figure 5 shows a maximum point of energy efficiency that depends on the fan speed. For the simulation model, the energetic optimum is a normalized Fan speed of $n_\mathrm{norm} = 0.87$ (compare Figure 5, blue).

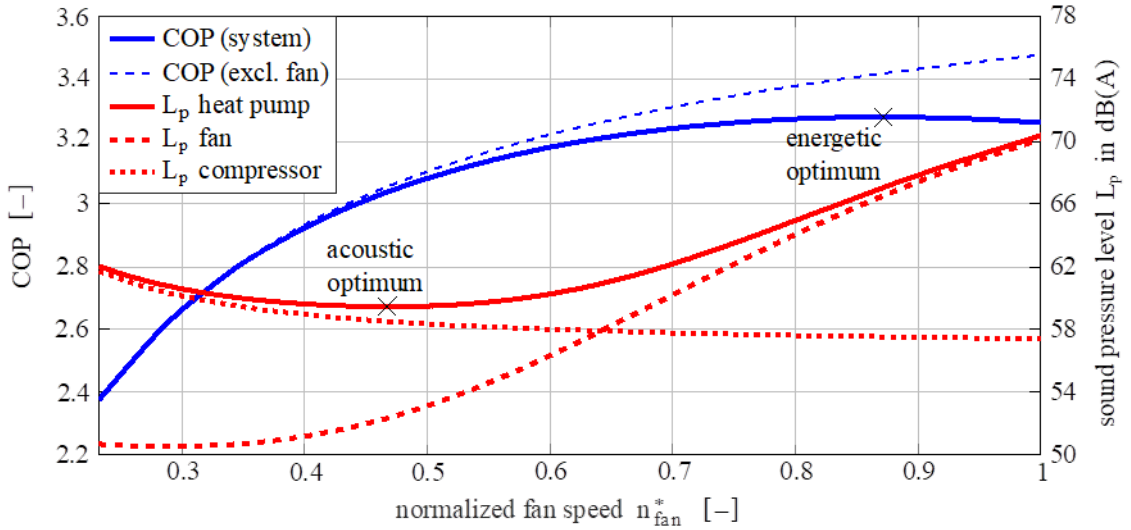


**Figure 5: Acoustic signatures of compressor and fan, as well as their sum as function of normalized fan speed, demonstrate the conflict between energetic optimal operating point and acoustic optimal operating point. [5]**

In the context of this work, energy-optimal refers to the provision of a heat output with minimal electrical energy consumption. It follows from the observation that the rated speed of the fan ($n_{\mathrm{norm}} = 1$) does not represent the energetic optimum. The varying speeds of the compressor and fan lead to different acoustic emissions from the heat pump. An increase in fan speed leads to an increase in the sound pressure level through the fan. The effect of the compressor is counteractive: As the fan speed increases, the compressor speed decreases and with it the emitted compressor sound level.

Both sound sources are calculated and logarithmically summed up. Since the components were measured individually and under the same structural conditions, this is permissible.

In this simulation, the acoustic optimum is at lower fan speeds ($n_{\mathrm{norm}} = 0.46$). Thus, the operating points for the acoustic and the energetic optimum do not coincide, resulting in a conflict of objectives. The position of optima differs by $\Delta n_{\mathrm{norm}} = 0.41$, which corresponds to 410 rpm for the selected fan. At the acoustic optimum, the system $COP$ is reduced by 7.6 % compared to the energetic optimum. The emitted sound level, however, drops about $\Delta L_{\mathrm{p}} = 7.74$ dB(A).

In addition, Figure 5 shows a Pareto effect between energy efficiency and acoustic emission:

The overall emission can be disproportionately reduced by a comparatively small deviation from the energetic optimum. For a standardised speed of $\Delta n_{\mathrm{norm}} = 0.7$ the $COP$ of the system is reduced from $COP = 3.27$ to $COP = 3.23$. This means a reduction in efficiency of 1.22 %. The acoustic emission drops from $L_{\mathrm{p}} = 67.2$ dB(A) to $\Delta L_{\mathrm{p}} = 62.2$ dB(A). This means that a very small reduction in energy efficiency can reduce noise emissions by about $\Delta L_{\mathrm{p}} = 5$ dB(A). This Pareto effect is used in the following sections in order to realize an energetic-acoustic optimal operation (EAO).

The respective optima are strongly dependent on the ambient temperature and the heat demand. This leads to the Optima shifting during heat pump operation.

To solve the conflict of objectives, a real-time adaptive optimization algorithm must therefore be selected. In addition, the method should be easy to implement and should not require complex

measurement technology (pressure sensors, mass flow sensors, etc.), in order to enable economical application in new heat pump systems.

One possibility here is model predictive control. However, this technology needs high level of model accuracy and simulation speed, which makes practical implementation difficult. For this reason, research on model-free adaptive optimizers has been intensified in recent years. This includes the extreme value controller ESC, which is implemented with a Kalman-Filter as gradient estimator.

### *The objective function*

In order to realize the compromise between energetic efficiency and acoustic emission in the simulation model, a corresponding objective function is required. The target function must be convex and should have constant gradients for computing performance. The latter enables a constant convergence speed and easier parameterization.

Ensuring an economic application in heat pump systems, it must be possible to determine the quantities used without additional measurement technology. The $COP$ is not suitable for evaluating the energy efficiency of the heat pump, for which the heat supply transferred at the condenser must be determined. In addition, all flow temperatures as well as mass flows must be known. Especially the measurement of the mass flow is complex and therefore expensive. Electrical power consumptions, however, can be measured easily. The acoustic emission of the heat pump is specified by the sound pressure level.

Combining both, we formulate the target function:

$$TF = \min a * \frac{\sum P_{\mathrm{el}}}{\sum P_{\mathrm{el,max}}} + (1 - a) * \frac{\sum L_{\mathrm{p}}}{\sum L_{\mathrm{p,max}}}$$

The left term contains energetic assessment of the operating point and the right term contains the acoustic information. For comparability, the terms are normalized to their maximum values. With the parameter a, which takes on values between zero and one, the operating point to be controlled can now be specified:

a = 1: Energy-optimal operating point

a = 0: Acoustic-optimal operating point

For a = 1 the ESC will converge to the energy-optimal solution, while for a = 0 the quietest operating point is set. For values 0 < a < 1 it is possible to continuously weight between energy-optimal and acoustically-optimal operating point, which is called energetic-acoustic optimal operation (EAO).

### *Variation of the weighting a during operation with different gradient estimators*

This section examines the ESC performance for different boundary conditions. For this purpose, a parameter is varied during the simulation, which results in a change of the target function. Applying ESC, we compare Kalman-Filter to RLS as gradient estimators.

A variation of the parameter *a* leads to a jump of the target function. A possible application is that the heat pump should be operated at night with lower sound pressure levels than during the day. For this purpose, the parameter *a* is varied during the day. Figure 6 shows an example of the fan speed

curve and the target function for abrupt changes of parameter *a*. The model is initialized with constant fan speed and after 200 s the ESC is activated.

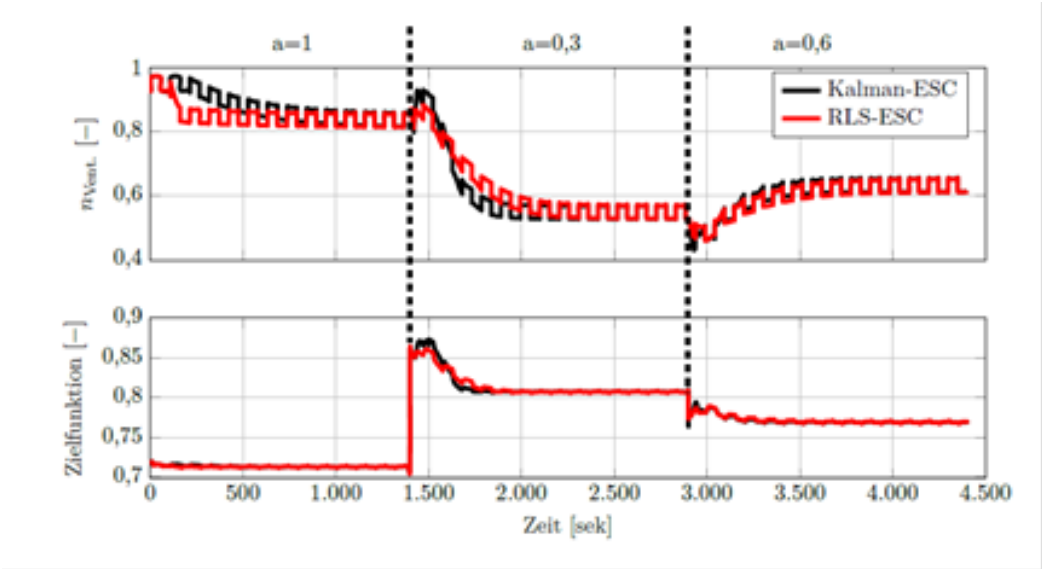


**Figure 6: Applying RLS-ESC and Kalman-ESC to investigate ESC performances to control the heat pump with changing boundary conditions. [5]**

First, the target function is used to determine the energy-optimal solution (a = 1). After 1400 s the weighting is changed to a = 0.3 and after a further 1400 s the parameter a is set to 0.6. It can be clearly seen that after both jumps of the objective function the normalized fan speed changes. This applies to both gradient methods as well as for each weighting change.

The behaviour is due to the fact that the gradient methods provide a gradient estimate of the states before and after the jump comparison and, based on this, a gradient estimate which is, however, inadmissible. For the Kalman-ESC this effect is higher, since the gradient estimation is only done through two data points. For the RLS-ESC, where a large number of past data points are included in the estimate function, the effect is less distinct.

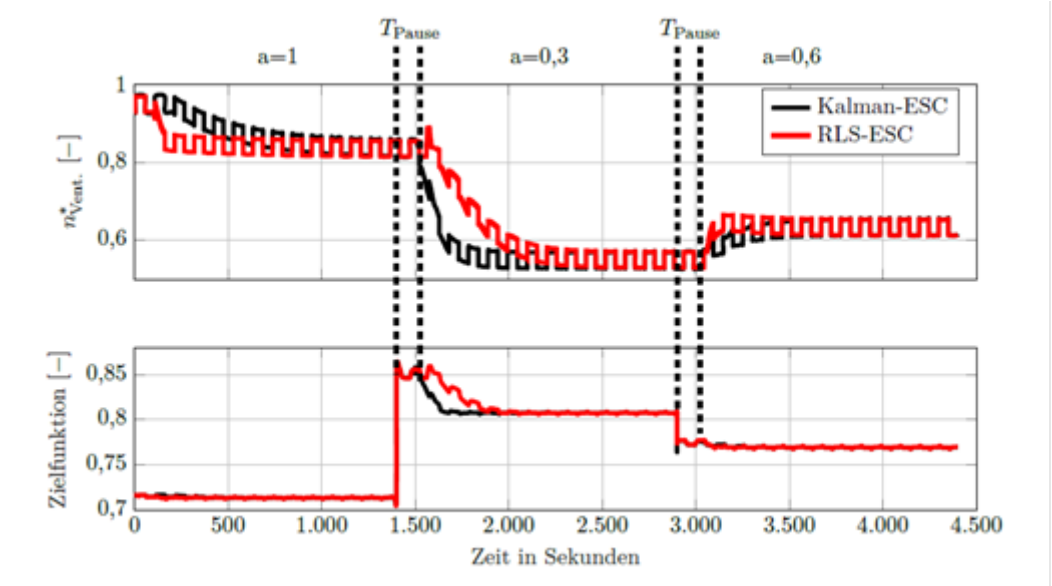


**Figure 7: Introducing a break time to increase robustness of ESC.**

Since the adaptation of the normalized fan speed against the optimization direction increases the convergence time of the algorithm, a procedure is implemented to prevent this effect. For this purpose, the ESC is stopped for one complete period of the perturbation signal $T_{\mathrm{Pert}}$:

$$T_{\mathrm{off}} = T_{\mathrm{Pert}}$$

During this time the gradient method collects information about the new optimization environment without changing the manipulated variable. The results of this additional rule are shown in Figure 7 for both gradient estimators. After a jump of the parameter *a* the fan speed initially remains constant for $T_{\mathrm{Off}}$. After reactivating the ESC, the speed for Kalman-ESC moves in the optimization direction. The RLS-ESC continues to change the speed for a short time against the optimization direction. In order to ensure the desired behaviour of the RLS-ESC, the algorithm has to be stopped for a longer time, which has a negative effect on the convergence time.

### Evaluation of the EAO approach

With the conflict between energetic efficiency and acoustic emission formulated as an optimization problem, applying ESC allows to control any conditions between energetic and acoustic optimum. This way, both user comfort and heat pump efficiency can be increased in a simulative manner. No additional measurement technology needs to be installed on the heat pump to run EAO method.

For the first time, acoustics can be implemented as a variable to be optimized. For this purpose, acoustic measurement data is coupled to the speeds of the fan and compressor. The challenges of the presented procedure are the implementation and parameterisation of the ESC on a real heat pump. Since heat pumps have long dead times due to the inertia of heat exchangers, the convergence time of the algorithm is limited. The convergence times achieved here are not yet representative due to the simplified dynamic modelling. Experiments need to prove that the convergence time of the algorithm is fast enough to ensure economical use.

The literature shows convergence times between one and three hours. However, as these depend largely on the distance between the initial manipulated variable and the optimum manipulated variable, it remains difficult to make a fair comparison. However, ESC leads to an improvement of the current state, even if the algorithm has not converged to the optimum yet.

In addition to the convergence time, the parametrization of the gradient estimator on a real heat pump is also challenging, since the dynamics of the parametrization process of the heat exchanger slow down over time. These dynamics were not realistically represented by the simulation model. The gradient estimator parameters used in this work will differ from test bench parameters.

It is expected that the frequency will have to be reduced in order to counteract the slow dynamics and a possibly bad controller design. Due to loss mechanisms, disturbances and measurement uncertainties, the course of the system output cannot be exclusively attributed to the perturbation of the manipulated variable. In order to quantify the influence of perturbations, the amplitude of the perturbation may therefore have to be increased.

## Modelling and simulation of frost as a transient acoustic phenomenon

As detailed in the second part of this report, the frosting of the evaporator represents one of the main noise sources amongst transient operations:

- The frosting itself gradually obstruct the evaporator, leading to an increased load and in turn increased noise of the fan.
- Eventually, the heat pump will trigger a defrosting cycle, which might not be as loud as normal operation, but whose transient and tonal character can lead to much annoyance.

In order to better understand and characterize this icing process on a tested heat pump, the Austrian Institute of Technology developed a dedicated model [6].

The parameter study includes different tube and fin temperatures, different mass flows through the heat exchanger and different boundary conditions on the air supply side of the heat exchanger, which influence the absolute water content in the supply air. The results of the symmetrical parameter study were used to reconstruct the behavior of the entire heat exchanger design.

For comparison, some experimental observations were conducted based on thermodynamic measurements for the thermal operating parameters of the heat pump, weight measurements using a scale and image acquisition techniques from standard cameras and thermal cameras to visualize ice growth and extract the frost layer thickness.

## Geometric model

A four-row heat exchanger including the volume between the heat exchanger and the fan was modelled. Using the experimental boundary conditions for an evaporating refrigerant, numerical simulations were performed on the entire heat exchanger assembly. Frost mass, increasing air flow velocities and pressure increase during subsequent freezing and blocking of the heat exchanger were additionally calculated for operation with a non-evaporating refrigerant, which ensures a linear temperature distribution along the refrigerant tubes. Temperature, flow field and frost layer were calculated with the Navier-Stokes solver OpenFOAM®, which was extended with a custom icing code. The fan was not modelled with its real geometry, but with a suitable boundary condition.

Two geometric models have been constructed: a complete heat exchanger model and a smaller fully symmetric part of the heat exchanger (Figure 8) for parametric investigations of the dependence of the frost accumulation on the fin temperature and the boundary conditions on the supply air side (temperature and humidity).

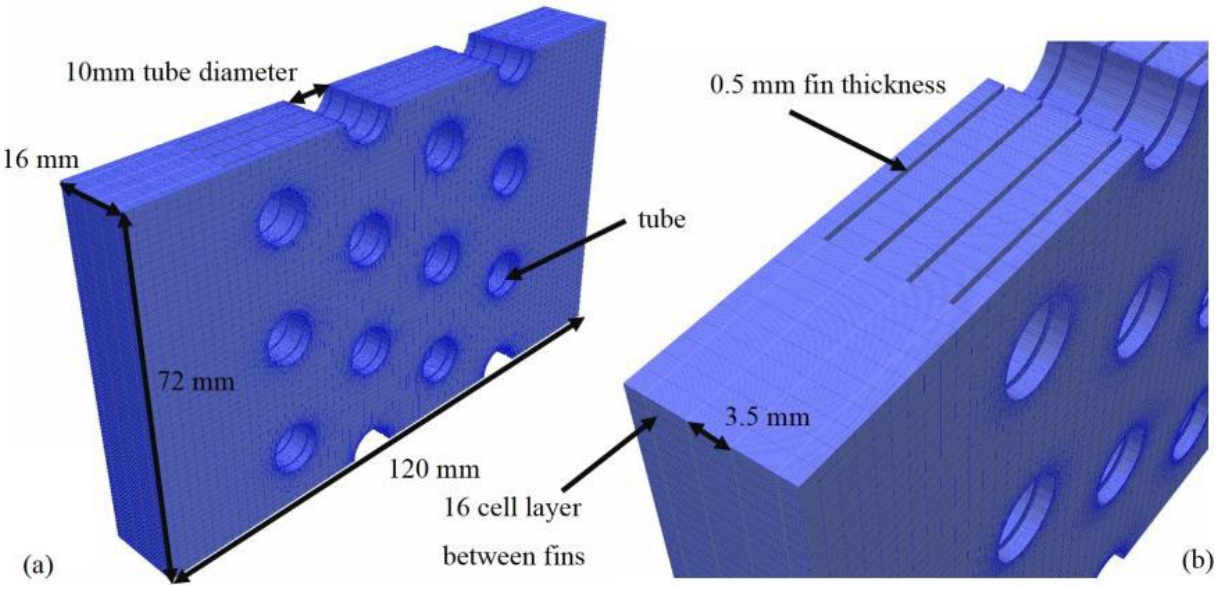


**Figure 8: (a) Symmetrical part of the heat exchanger with a total depth of 120 mm containing all 4 tube layers in the direction of flow. In this model there are 4 fins and 12 tubes (b) Detailed view showing the computing network with 16 cell layers between 2 ribs.**

The boundary conditions include the temperatures at the fin, tubes and the inlet and outlet side of the heat exchanger assembly. Furthermore, velocity profiles on the discharge side must be set at the location of the fan. Humidity was set on the air supply side.

## Icing model

The key data of the icing process considered in this paper are outlined in Figure 9. During this process, humid air flows over a cold wall, and a frost zone is created by the heat and mass transfer over the frost surface.

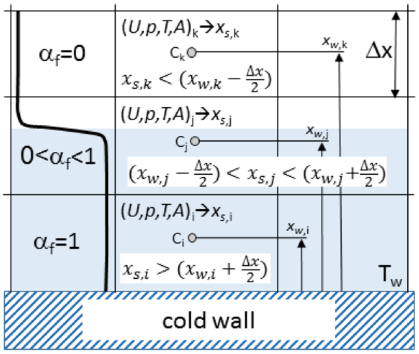


**Figure 9: The parameters of the icing process [6].**

The analysis of frost growth over a cold wall starts with the equilibrium of the total mass flow of water vapour, which is transferred from the surrounding moist air over the frost surface into the frost zone. The total mass flow, which comes from the surrounding humid air, can consist of two parts: one that diffuses into the existing frost zone and changes its thickness, and the other that compresses the frost.

Combined to an empirical function of the frost density depending on the frost surface temperature, and assuming that the frost properties are constant over the entire frost zone, one obtains the frost growth rate. This growth rate in turn is used to update the actual thickness of the frost zone at each time step.

The heat balance over the frost surface indicates that the total energy transferred from the surrounding humid air consists of the conduction through the frost zone and the latent sublimation heat within the frost zone. By combining with the expression of total mass flow of water vapour and rearranging, the temperature of the frost surface is obtained.

The icing model is implemented in such a way that frost growth is derived from the local flow properties taking into account the spatial and temporal distribution of the relevant humid air flow variables: velocity U, temperature T and absolute humidity A. The entry of frost on a cold wall is controlled by the nucleation theory. After this initial phase, however, the frost surface moves in the direction normal to the wall, and the newly formed layer between the cold wall and the frost surface is treated as porosity: There the humid air flow is blocked and the swell/sink term is introduced into the transport equations for temperature and absolute humidity.

For each cell in the numerical network, the frost zone is quantified by the ratio of the locally calculated frost thickness xs and the height of the cell Δx. Thus the defined quantity has a value between zero (the cell is frost-free) and one (the cell is filled with frost). Consequently, according to Darcy's definition of pressure drop for flows through porous media, the blockage of the humid air flow will be relatively small when the frost starts to fill the cell and grow exponentially when the cell is fully frozen. This is reflected in the results when considering the total pressure drop: It grows slowly, as the frost thickness above the slats is relatively small, and shows a sudden jump, as the

majority of the cells along the slats become almost full of ice (this behavior is reduced when the mesh is refined).

The simulations with the overall heat exchanger models followed a two-stage approach. In the first step a Laplace calculation was performed to solve the heat conduction equation for the distribution (diffusion) of the tube temperatures on the fin surfaces. Then the temperatures at fins and tubes were determined and the Navier-Stokes solver was started with the above presented icing code (and used for the symmetric simulations).

## Simulation results

Running the model on a powerful computing cluster, numerous results on the icing factors and their influence as well as on the icing consequences could be obtained.

As expected, during icing, more and more volume is filled with frost (Figure 10). As a result, the pressure also rises, which ultimately leads to a sharp drop in pressure across the heat exchanger. This in turn leads to an increased load for the fan, which is likely to get louder. As more and more volume is occupied by frost, the flow velocity increases so that the mass flow can remain constant, likely creating more aeroacoustic disturbance as well. This mass flow must of course be provided by the fan. Because fans normally operate in operating curves (instead of providing a constant mass flow), which have a non-linear dependency between pressure and mass flow, the flow velocities will eventually decrease in severe frost conditions.

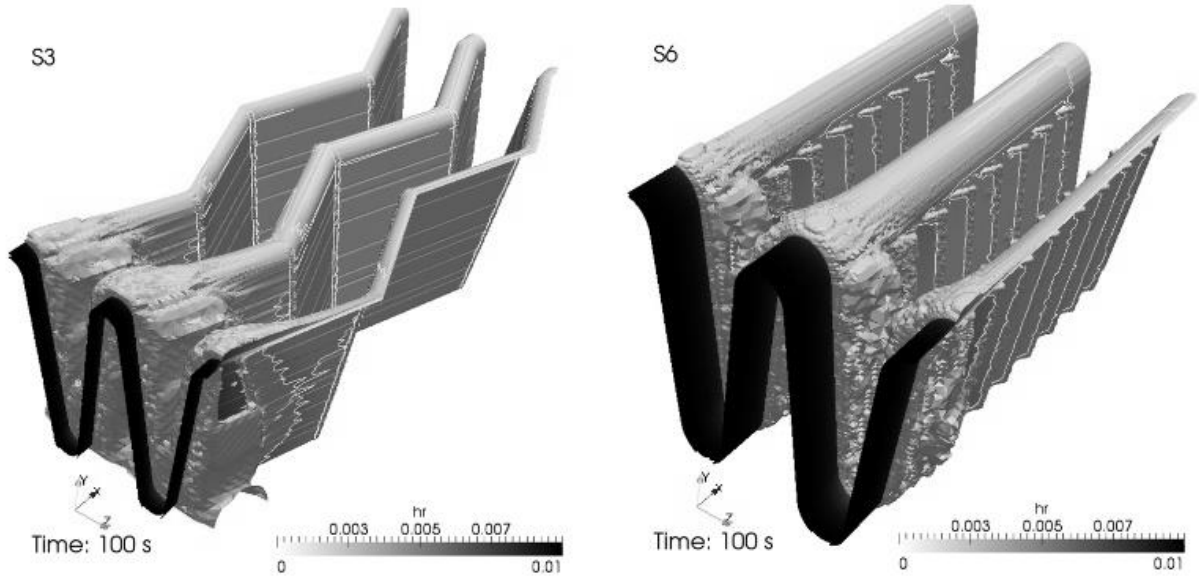


**Figure 10: Temporal behaviour of the ice build-up on a small symmetrical section of the heat exchanger. At the top, the flow velocity is shown, below the pressure loss with gradual icing [7].**

In addition, the simulations with the overall heat exchanger showed the inhomogeneity of the frost repartition on the heat exchanger, due to the variation in local flow velocity and the repartition of the different phases of the refrigerant in the circuit. Such irregularities are likely to contribute some more to aeroacoustic disturbances of the air flow.

Finally, the strong influence of several operating factors on the icing speed could be demonstrated:

### *Fin and tube temperature*

As shown in Figure 11, the change in fin and tube temperature has a great influence on the speed of the icing process, and therefore on the pressure drop.

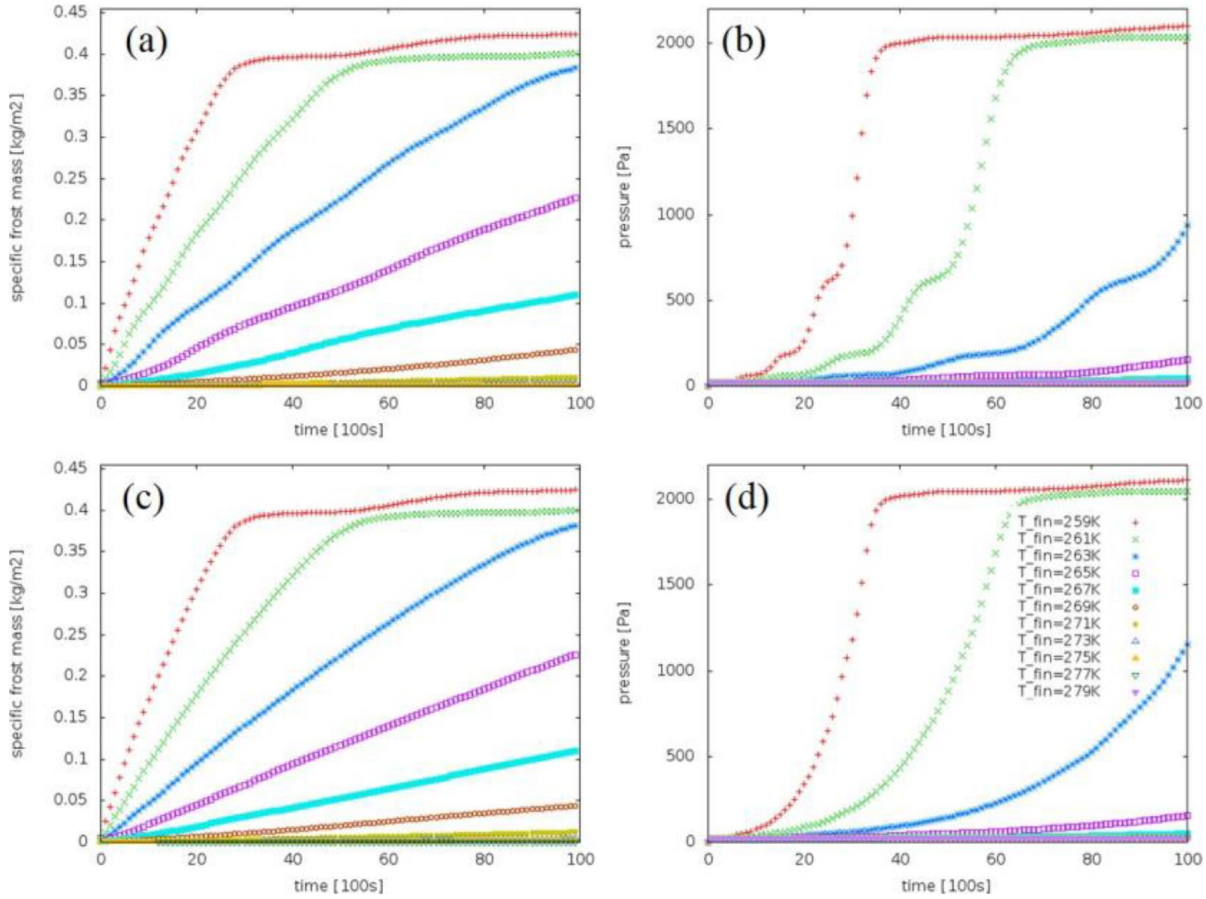


**Figure 11: Accumulated frost mass (left) and corresponding pressure drop (right) for different fin and tube temperatures at a constant temperature of 275K, a constant relative humidity of 90% and a velocity of 2m/s on the air supply side; a,b: Results from simulations with 8 cell layers between fins; c,d: calculations with 16 cell layers between the fins.** [8]

On Figure 12, it is easy to see that icing is already a much slower process when the fin and tube temperatures are increased by 2 K from the reference case.

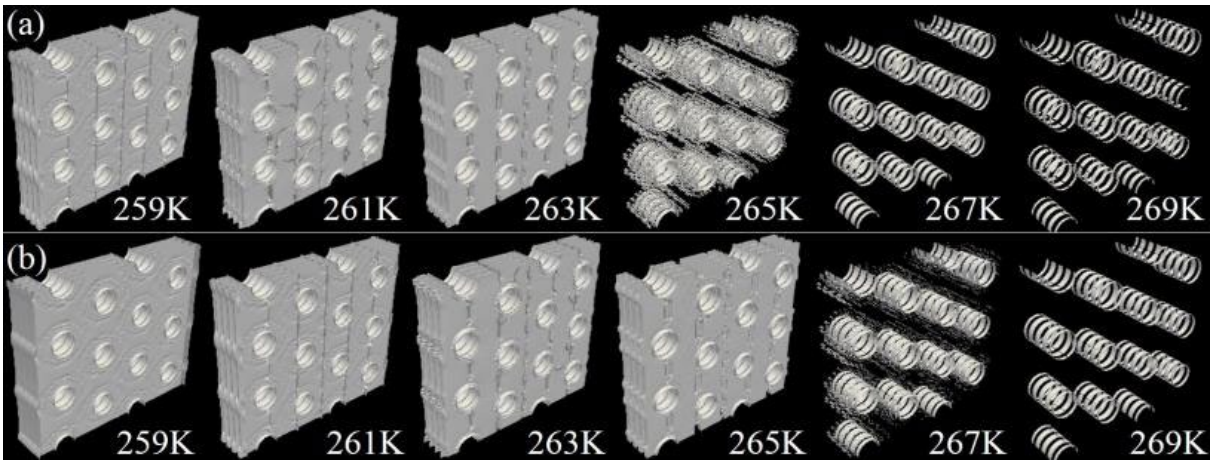


**Figure 12: Accumulated frost mass for different fin and tube temperatures from 259 K (left) to 269 K (right). The following boundary conditions are defined on the air supply side: Temperature 275 K, relative humidity 90%, speed 2m/s. (a) Comparison to time 3000 s, (b) Comparison to time 5000 s [8].**

### *Flow Velocity*

The change in flow velocity also has an influence on the frost behaviour. This is illustrated in Figure 13 by showing the frost coloured by the velocity for speeds of 0.5 m/s to 3 m/s for temperature boundary conditions similar to the reference case.

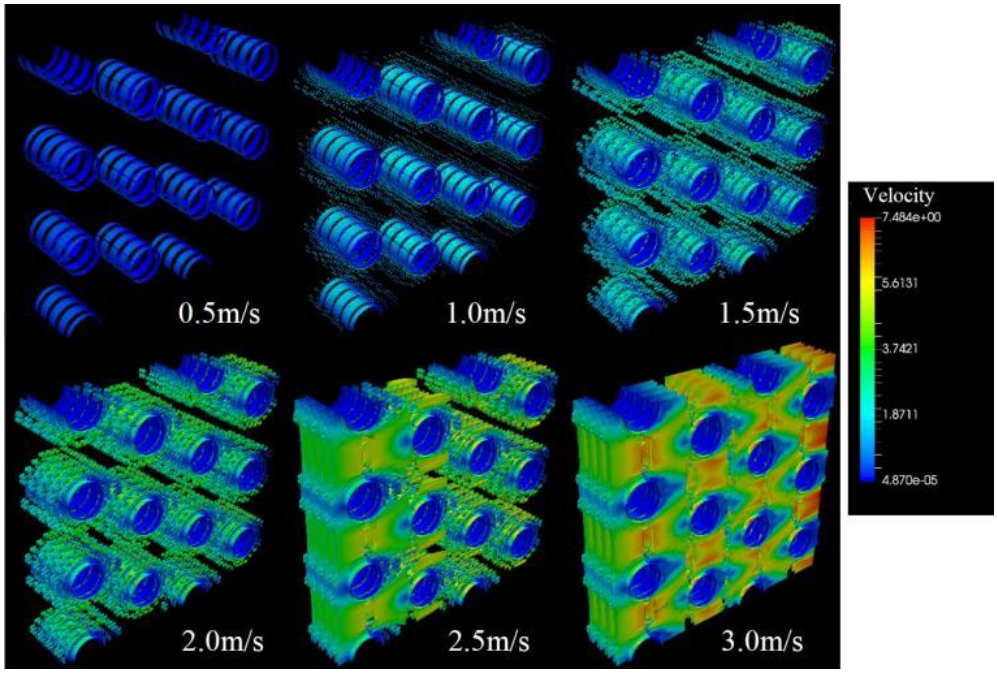


**Figure 13: Accumulated frost mass for various air supply speeds from 0.5 m/s to 3 m/s. The following boundary conditions are defined on the air supply side: Temperature 275 K, relative humidity 90 %. The pipe and fin temperatures are fixed at 263 K. The frost zone is colour-coded by the velocity size. The time for all 6 figures is 1800 s [8].**

### *Temperature and humidity on the air supply side*

The relationship between frost mass and pressure loss and the temperature on the air supply side is shown in Figure 14. Increasing the temperature on the air supply side increases the amount of water available for the formation of frost on the fin and tubes, so that clogging of the heat exchanger is achieved much faster at higher temperatures on the air supply side.

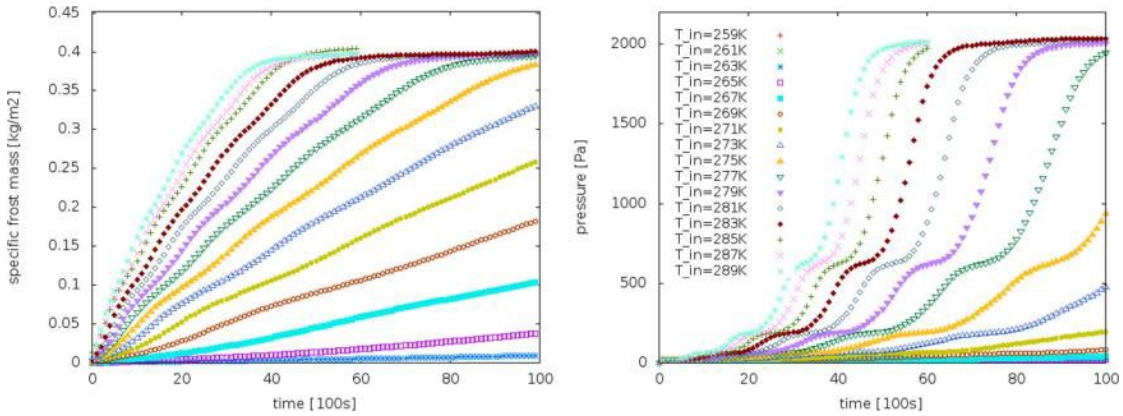


**Figure 14: Accumulated frost mass (left) and corresponding pressure drop (right) for different temperatures on the air supply side at a constant relative humidity of 90% on the air supply side and a constant fin and tube temperature of 263 K. The velocity of the air supply side is fixed at 2 m/s [8].**

Figure 15 shows the relationship between frost mass and pressure loss when the relative humidity on the air supply side changes from 10% to 100% at a constant temperature on the air supply side of 275 K - thus changing the absolute humidity (water content) there. The temperature on fins and tubes was kept constant at a value of 263 K as set in the reference case. A similar behaviour to the variation of the temperature on the air supply side can be observed. However, the frost times at 100% humidity at 275 K shift by a factor of about two compared to a calculation at 90% humidity at 289 K according to the specified absolute water content.

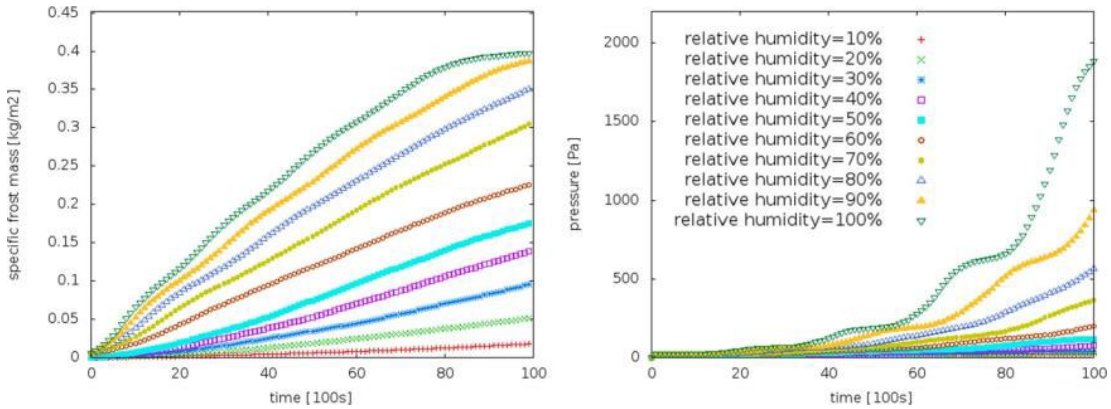


**Figure 15: Accumulated frost mass (left) and corresponding pressure drop (right) for different relative humidities on the air supply side and constant fin and tube temperature of 263 K and a constant air supply side temperature of 275 K. The air supply side velocity is fixed at 2 m/s [8].**

In conclusion, the cumulative frost layer observed in the numerical data can be compared with experiments. Sharp structures are observed in the initial frost state and are smoothed more and more during subsequent frost formation of the area between the fins.

The ability to predict the heat exchanger performance including icing without multi-core overall simulation models is crucial for the introduction of these icing models into the development chain of heat pump heat exchangers, because if the geometry of the heat exchanger (e.g. distance, depth and curvature of the fins) changes, only the symmetric simulations for a given set of boundary conditions have to be performed.

## Other system modelling tools for transient operations

As far as the literature review could assess, all the other relevant modelling tools to analyse the acoustic impact of different operating conditions are also restricted to the effect of one component or transmission path, as a consequence of their higher dimension and more complex physical model, leading to high computational loads.

Amongst those methods, some are already proven techniques with maturity, such as:

- *Finite Elements Method (FEM)*, applied to structural dynamics or fluid dynamics.
- *Boundary Element Method (BEM)*, essentially to compute the radiated airborne sound out of a solid vibrating surface.
- *Computational Aero-Acoustics (CAA)*, used to model the sound emission arising from airflow turbulences (therefore mainly for steady state).

Some other techniques only recently reached a development state allowing for use in complex geometries. For example, models based on the structure-borne sound intensity can be used in the time domain to describe transient phenomena accurately, but only work so far for thin plates or shell elements [9, 10]

# Sound emission during transient operation

It is generally considered that the two main noise sources of a typical air/water heat pump are the operation of its fan and that of its compressor, both of them being likely to reach a higher sound level the faster they operate, i.e. the bigger the load.

Even though transient operating processes either originate from those two components at lower speeds, or from secondary sources whose emitted sound power is comparatively lower, the suddenness or evolutive character of those transient noises gives them a decisive role in our perception of the acoustic annoyance of such appliances.

It will first be looked into the physical processes at the origin of the most significantly noticeable transient noises.

## Acoustics of transient heat pump operation

By definition, transient heat pump operations are the evolutive processes and those whose duration is limited in time. Consequently, the main reasons to reach such states are:

- Events regarding a change in the requested capacity of the heat pump:
    - Start and stop processes (including the intermittent switching of models without inverter control)
    - Load change and inverter modulation
    - Hot water tapping
- Events regarding a change in the conditions to reach such desired capacity:
    - Change of external conditions like the progressive frosting of the evaporator
    - Change of ambient temperature
- Events as part of a defrosting cycle
- Events regarding an independent secondary source, such as the operation of the circulation pump.

It is worth noting that some evolutive processes take place on such a big time scale, that they will be explored in a subsequent part of the report.

### Short term transient events

#### On/Off switching and inverter control

During on and off switching, the rotating components travel through a continuity of rotational speeds (possibly stepwise in the case of inverter control).

For each rotational speed, the emitted spectrum has been observed to be virtually equivalent to those of corresponding power/rotational speed in steady state [11] (cf. Figure 16).

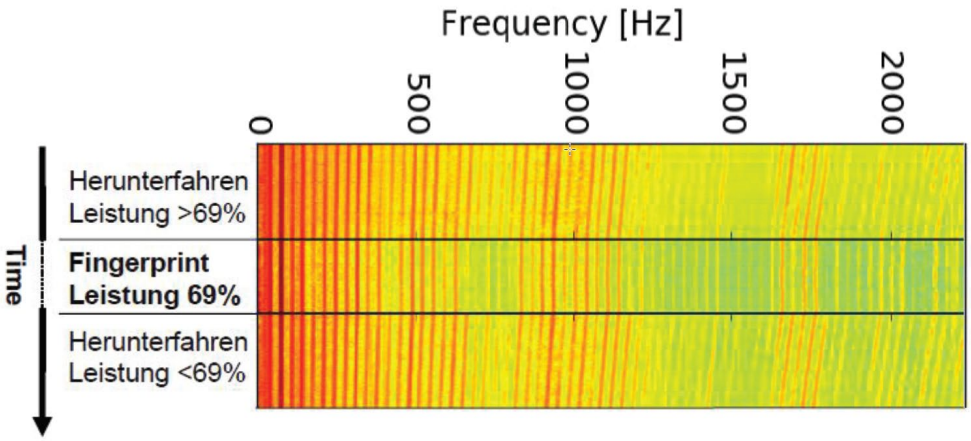


**Figure 16: upper and lower parts represent the acoustic signature of a compressor shutdown, while the middle stripe is that of its steady state operation at 69% part load. From [11].**

## Frosting

The latent heat being taken off the ambient air by the vaporization of refrigerant in the evaporator leads to condensing of the air humidity on the outside surface of the component.

While operating at low ambient air temperatures, the evaporator will reach such low temperature that the condensed water will gradually freeze at its surface. In turn, the frosted water will progressively obstruct the interstices between the fins of the evaporator (Figure 17), leading to an increase of the fan load away from its optimal efficiency. Finally, this contributes to deteriorate the fans acoustical behaviour.

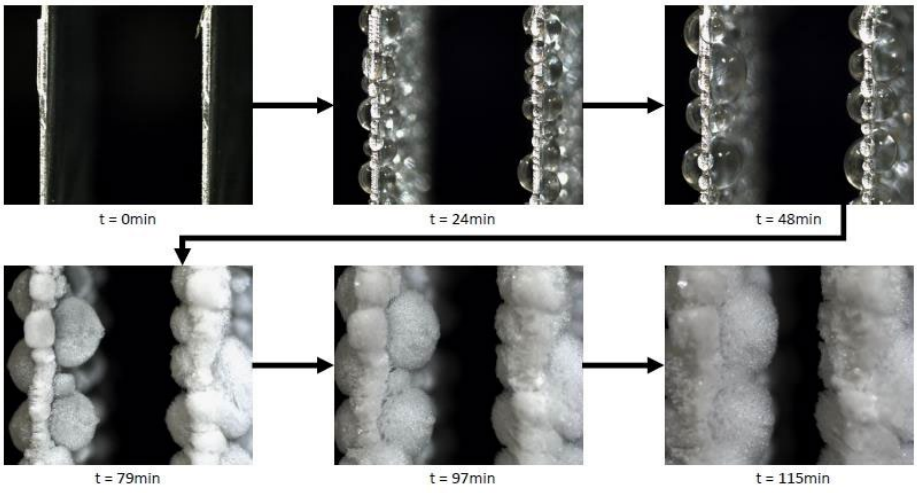


**Figure 17: Frost accumulation on two heat exchanger fins [8].**

At the example of Figure 18, the typical time scale of such evolution is of the order of an hour, depending on many parameters such as temperature, load, shape and size of the evaporator, type and capacity of fan, etc... It is possible to apply anti-ice coatings to delay the ice build-up of 10% and also obtain changes in defrost behaviour of the heat exchanger.

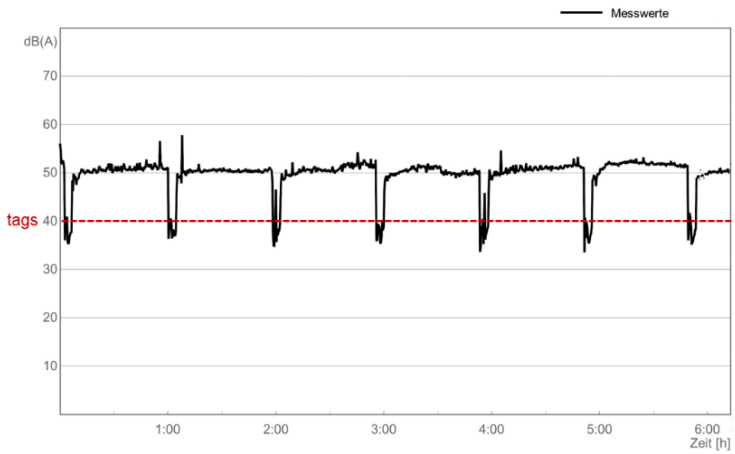


**Figure 18: Time evolution of the SPL of heat pump under operation. The level sinks every hour or so for defrosting cycles. From [12].**

During experiments at AIT, the effect of icing on the sound power level proved to account for approximately 2 - 4 dB(A).

To remediate to this predicament, the heat pump will enter in a defrosting cycle, which can be considered as the main succession of transient operating state in the function of air heat pumps.

### Defrosting cycle

The defrosting cycle happens in several steps, usually all several dB quieter than the normal operation around full capacity (see the detail of one cycle in Figure 19 or the regular drops of SWL in Figure 20):

- The fan and compressor shut down (the compressor of some models will just significantly slow down).
- The 4-way valve is operated to reverse the circuit starting at the compressor output, changing the pressure proportion in the different parts of the cooling circuit, which can lead to a strong hissing of the electronic expansion valve (EEV) when opening.
- The compressor accelerates again up to a limited speed.
- After the temporary role of condenser of the frosted evaporator has warmed it up sufficiently to allow full defrost, the compressor is shutdown (/slowed down) once more
- The 4-way valve is operated again, back into its initial position.
- (optionally, the fan operates once in reverse direction in order to evacuate the condensate, which could otherwise freeze back on its blades and affect its function)
- Finally, compressor and fan start again and accelerate up to their normal operating speeds.

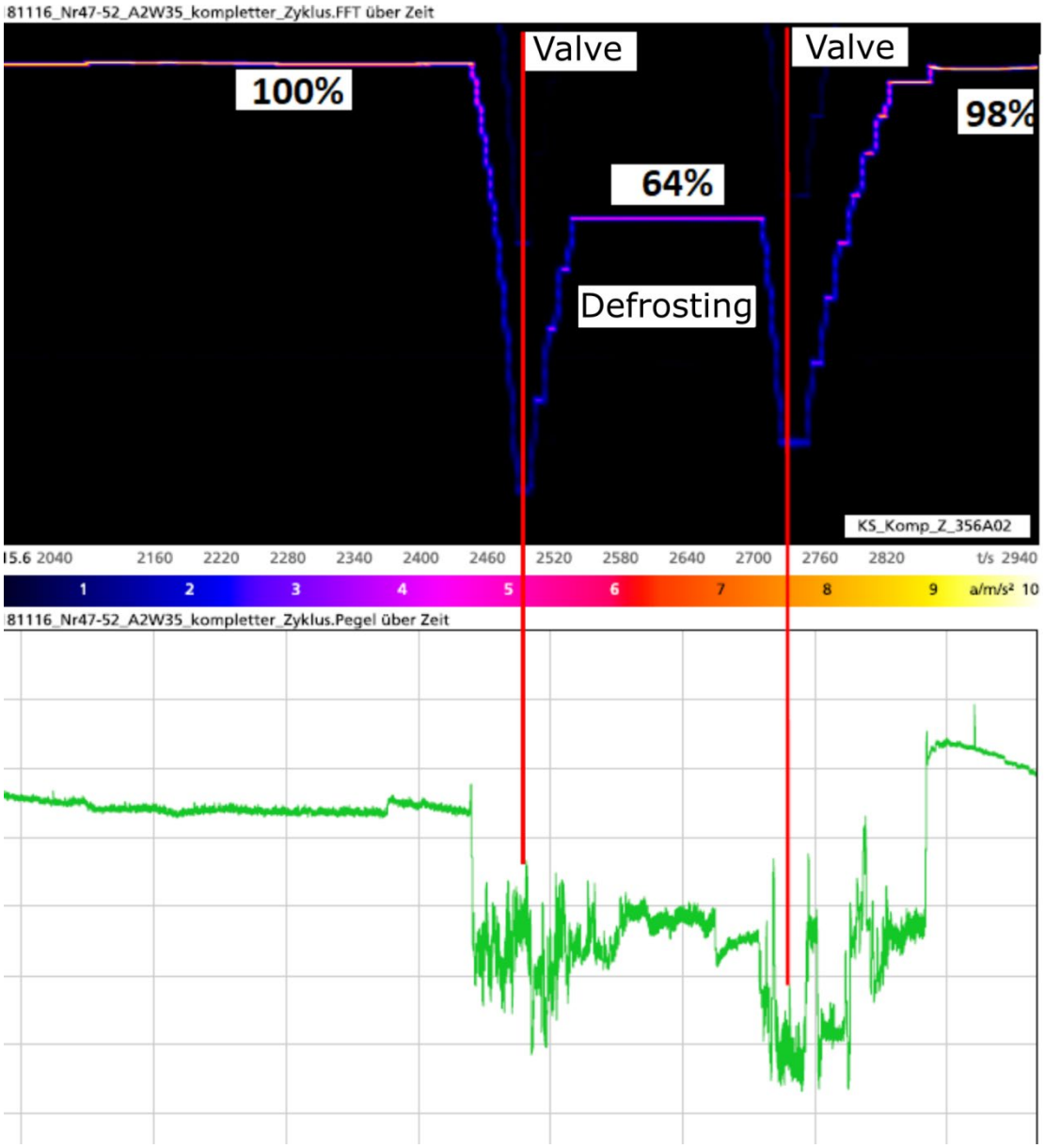


**Figure 19: Time evolution of a defrosting cycle, as measured at Fraunhofer ISE. The upper part shows the rotational speed of the compressor (acceleration sensor) and the lower part represents the global SPL, including brief events like the switchings of the 4-way valve.**

Along with anti-ice coatings, the defrost behaviour of heat exchangers can also be improved by a slight tilt of the fins, so that the condensate gets easily and entirely evacuated.

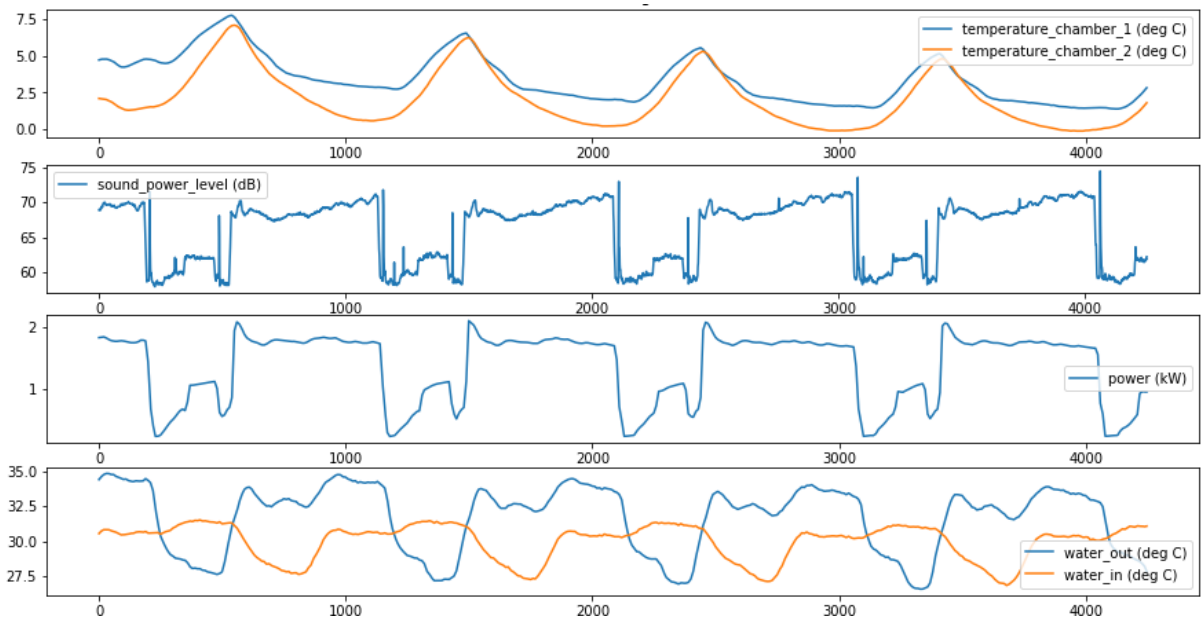


**Figure 20: Time history of important climatic chamber data. The defrosting cycles can be observed each 1000s or so, with a drop of the A-weighted sound power level. Short peaks are to be seen when the 4-way valve switches (source AIT).**

## Reverse Cycling

In order to ease the compressor load, refrigerant distributors can feature an intake/outlet asymmetry and be optimized for the normal operation of the heat pump.

As a result, one might observe a proportionally higher fluid-borne noise during defrosting, where the refrigerant usually flows in reverse direction through the evaporator and its refrigerant distributors.

## DHW Tapping

Heat pumps being used to provide domestic hot water (DHW) are usually put under high loads, as its target water temperature is usually around 55˚C instead of some 35˚C for floor heating.

Therefore, the tapping of a high amount of DHW will lead to a sudden decrease of the water temperature in the tank, thus abruptly increasing the load of the heat pump to maintain the reservoir at the desired temperature and ensure no DHW shortage occurs.

## Circulation pump

Like compressors in previous times, most water or brine circulation pumps nowadays have a binary mode of operation, leading to the sudden appearance and disappearance of the associated noise emission.

This noise is usually low enough to be negligible if other components of the heat pump are in function.

## Long term transient events

### Example of the ageing of elastomer grommets

Elastomer grommets used as damping material to dampen the structural dynamic excitation of the compressor display a complex set of properties depending on many parameters such as the excitation frequencies, the amplitude and direction of the displacements, the operating temperature, etc…

As reported in [13] , the mechanical properties of such materials are likely to evolve over time, and especially to degrade if subjected to high temperatures, then featuring an increased sensitivity to high amplitude vibrations.

As a result and with compressors usually reaching over 80˚C in normal operation, the general characteristics of the transmitted structure-borne sound can vary over long periods of time, thus changing the global characteristics of the radiated air-borne noise.

## Investigating time dependent acoustic signatures

In this part, one will try to characterize the acoustic signature of the different transient operations previously presented

### Frosting/Defrosting

- During the whole defrosting cycle, the fan isn't in operation, until the heat pump starts again towards normal operating state, and at the exception of advanced control strategies where the fan operates once in reverse direction in order to evacuate the condensate, which could otherwise freeze back on its blades and affect its function.
- As the compressor is shut down and started again, it gradually goes through all the intermediary excitation frequencies, some of which are likely to enter in resonance with the vibrating modes of the heat pump structure. With most modern compressors featuring an inverter, a measure to avoid such predicament is to use control strategy so that the compressors speed increases in steps and jumps quickly over the troublesome frequencies.
- Figure 21 shows the aeroacoustic effect of turbulence on the total radiated power in the case of a frosted evaporator.

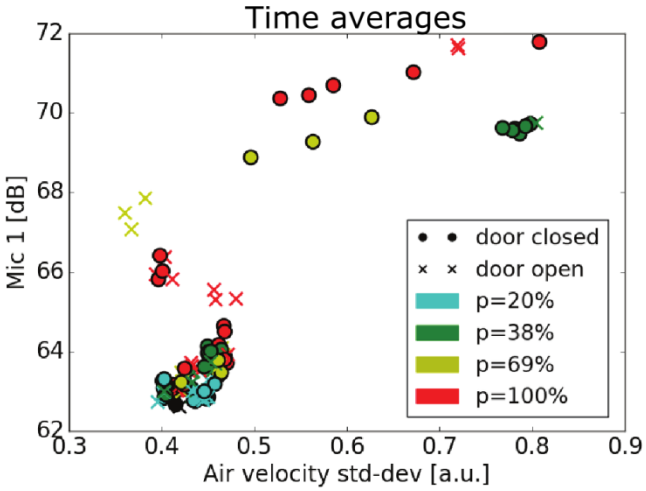


**Figure 21: Measurements with high values for turbulence and SPL coincide with the high frosted states p of the evaporator. From [11].**

- Figure 22 exemplifies the high acoustical impact that frosting can have through the increase of fan load: the air/water heat pump SPL is 11dB lower after defrosting.

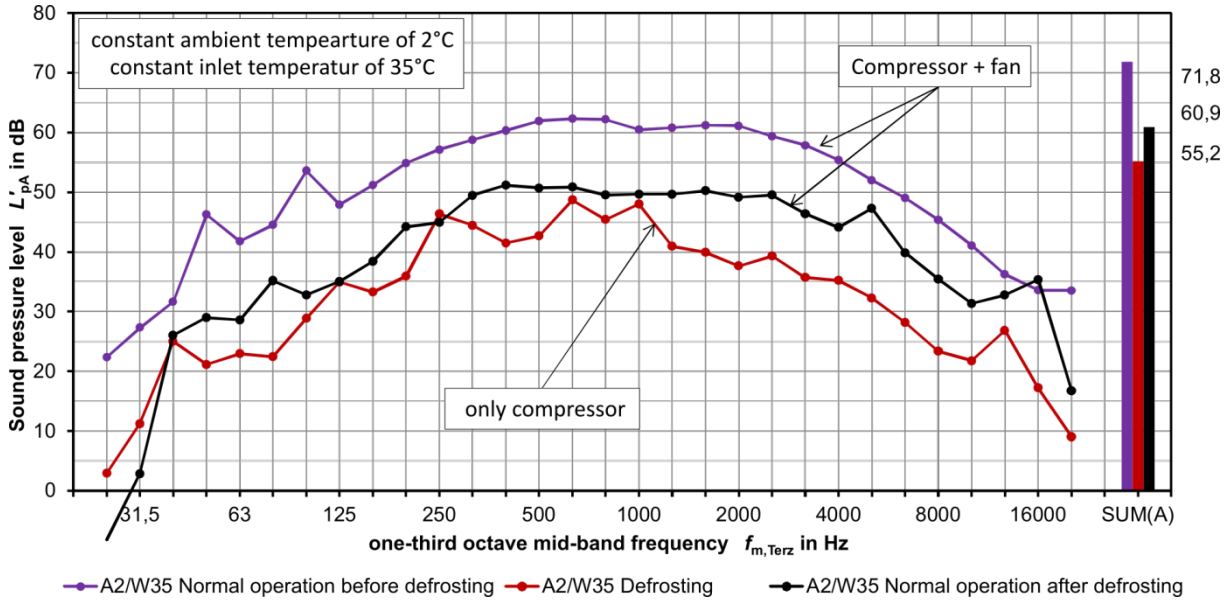


**Figure 22: SPL of a heat pump before (purple), during (red), and after (black) defrosting. From [14].**

- Similarly, Figure 23 shows the increase of SPL through frosting of the evaporator.

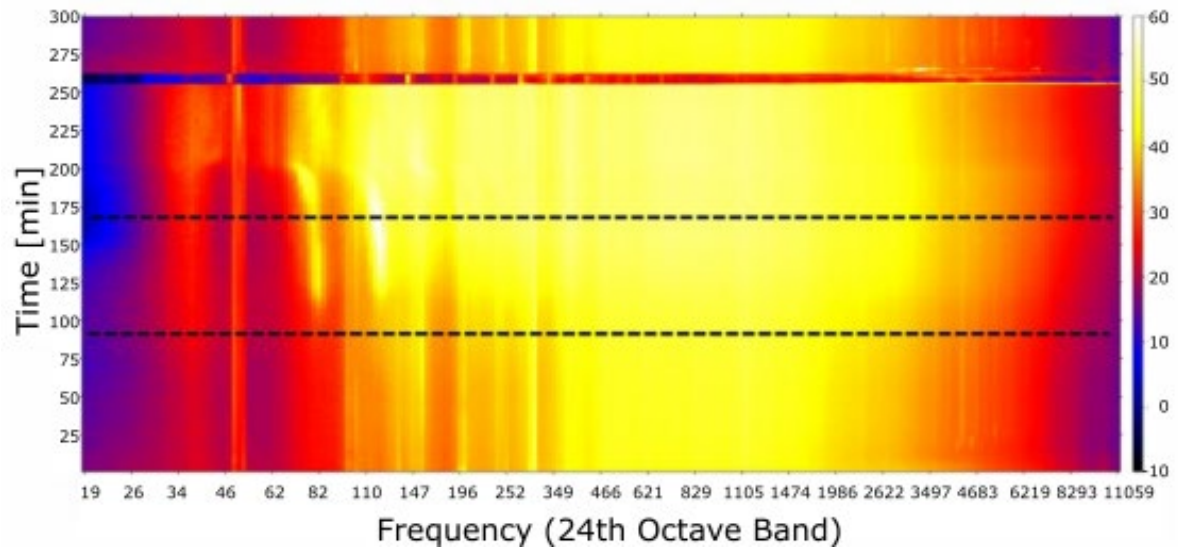


**Figure 23: Evolution of acoustic spectrum during frosting phase. The SPL increases of 8dB in the time between the 2 black lines. From [8].**

- Another frost example and its acoustical characteristics are depicted in Figure 24

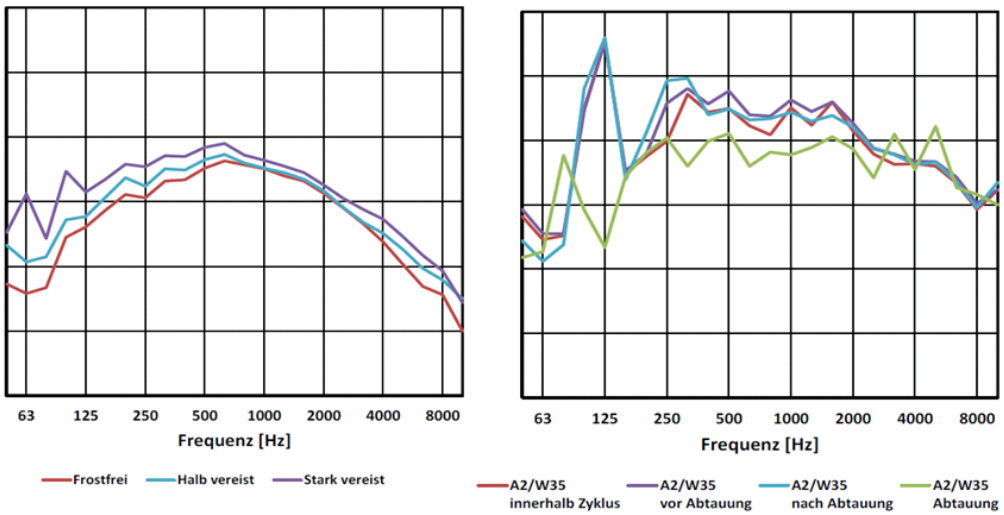


**Figure 24: Influence of frost of the evaporator (left) and assessment of defrosting noises (right). Fraunhofer ISE/IBP internal measurements.**

## Opening of the EEV

Figure 25 shows the brief hissing sound of the electronic expansion valve when opening. The delay between the microphones indicates the internal location of the sound source, whose excitation must mainly travel along the copper pipes of the cooling circuit.

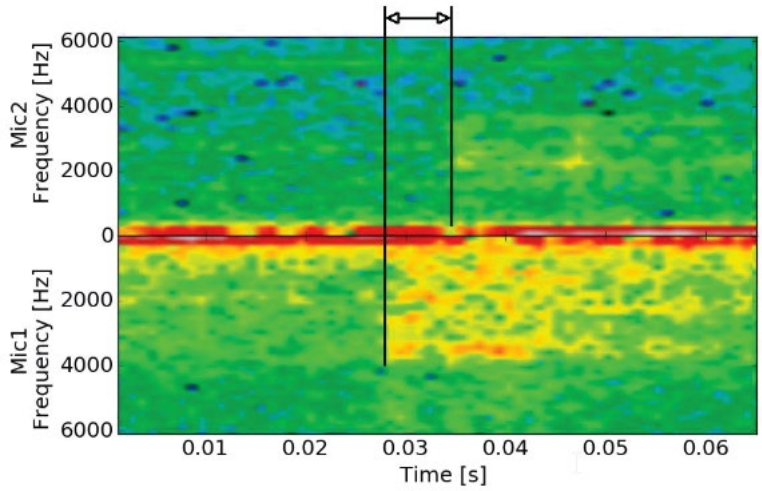


**Figure 25: Signature of the hissing noise from the opening of the EEV. From [11].**

## Switching of the 4-way valve vs time delayed operation

It has been experimentally demonstrated in [15], that idling before defrost could contribute to reduce the noise emission from EEV and 4-way valves (Figure 26). Furthermore, leaving the fan on and the EEV open while introducing a time delay to equilibrate internal pressure displays no significant loss of thermodynamic efficiency.

| | Reference | 60 s idling | 120 s idling |
|---|---|---|---|
| Heat capacity (relative reference) | 4.15 kW | 4.08 kW (98.4%) | 4.01 kW (96.8%) |
| COP (relative reference) | 3.21 | 3.21 (99.8%) | 3.20 (99.6%) |
| Noise reduction (average level) | – | 5 dB | 8 dB |
| Noise reduction (maximum level) | – | 7 dB | 12 dB |

**Figure 26: Time delay before defrost cycle contributes to reduce the hissing noise from 4-way valve and EEV. From [15].**

# Dependency on the type of heat source, and the temperature and load levels

In this section, it is investigated to which extent the noise emissions of stationary heat pump operation vary with:

- the type of heat source
- the type of heat sink
- the type of operation
- their control strategy

## Different heat sources

Several technologies (compression, adsorption…) and many variations come under the heat pump term. Nevertheless, compression heat pumps with air or ground as heat sources represent an overwhelming majority of the devices. Air is used for air-to-water and air-to-air heat pumps (including exhaust air heat pumps) and liquids (mostly glycol-water mixtures) is used for ground-source heat pumps. Ground source heat pumps exist in two variations, depending on their kind of ground circulation (Figure 27).

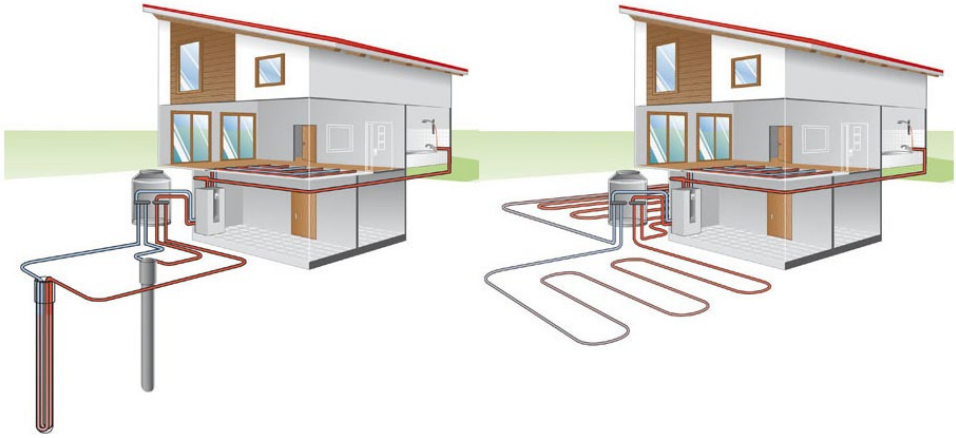

**Figure 27: Liquid source (or ground source) heat pumps come in two different kinds of brine circulation in the ground.**

Whereas a ground-source heat pump usually comes as a single indoor unit and only features a comparatively quiet circulation pump as noise source on top of its compressor, an air source heat pump consists of two main noise sources: its compressor and its fan, which normally come as integrated components in the outdoor unit.

An air-to-air split heat pump consists of both an outdoor unit and an indoor unit, the latter featuring an additional fan as only significant noise source.

Mainly because of the above-mentioned differences in characteristics, the noise level of a liquid source heat pump is comparatively lower than that of an air source heat pump, the dominant noise contribution only coming from the compressor.

Furthermore, the temperature gap between flow and return flow is bigger for air than for liquid source. As an example, in terms of average climate condition, a typical air source heat pump must

supply full heating demand at the lowest air temperature of -10°C (bivalent temperature). In comparison and for the same climate condition, the liquid source heat pump must supply full heating demand around 0°C liquid temperature. It should also be noted that the air temperature undergoes much more variations throughout a day, which forces the heat pump to vary its operation and makes it hard to run around an energetic or acoustic optimum at all times.

For a certain design capacity, this means that either the size of the compressor of an air source heat pump has to be larger or it has to run with a higher speed than that of a liquid source heat pump. In both cases this will likely render the air source device louder.

In the following example from internal measurements of the Danish Technological Institute (DTI) (see Table below and Figure 28), the heating capacity of the air-to-water heat pump is 9% lower than by the capacity of the liquid-to-water, while its sound power level is 18 dB higher than that emitted by the liquid-to-water heat pump.

| | | Air-to-water heat pump | Liquid-to-water heat pump |
|---|---|---|---|
| Heating capacity | kW | 5.44 | 6.0 |
| COP | - | 2.65 | 4.3 |
| Power input | kW | 2.05 | 1.4 |
| Outdoor heat exchanger inlet | °C | -10.0 | 0.0 |
| Outdoor heat exchanger outlet | °C | - | -3.0 |
| Indoor heat exchanger inlet | °C | 30.0 | 30.0 |
| Indoor heat exchanger outlet | °C | 35.0 | 35.0 |
| Sound power level | dB(A) | 65.0 | 47.0 |

It should also be noted that the power input is 46 % higher for the air-to-water heat pump, the difference likely coming from a higher load, volume or operational speed of the compressor, in addition to the power consumption of the integrated fan.

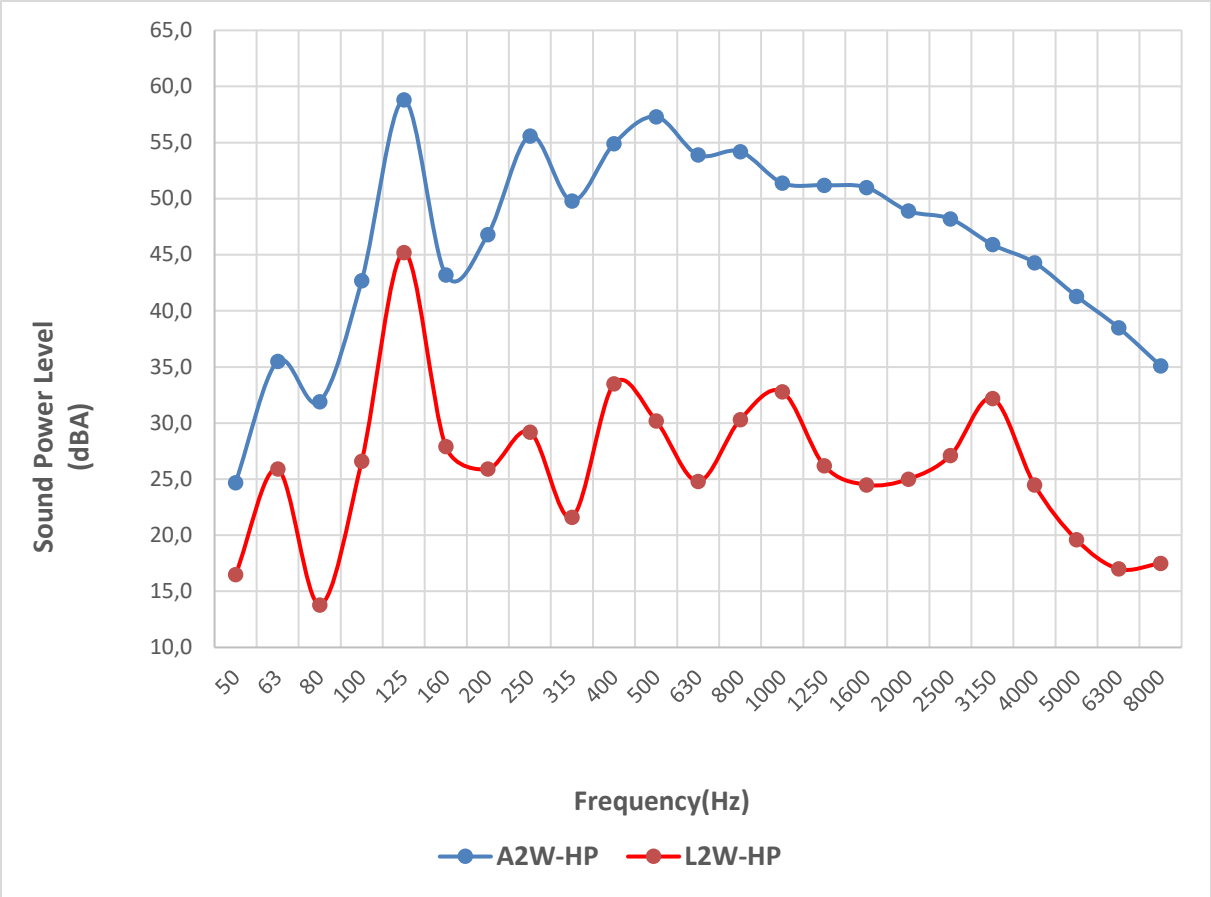


**Figure 28: Sound characteristics for an air source and a ground source heat pumps of similar capacity and at similar load. (source DTI)**

## Different heat sinks

A domestic heat pump designed for a floor heating system or a radiator heating system must supply a water temperature of 35°C at design temperature, respectively 55°C. When this heat sink temperature increases for the same source temperature (e.g. an outside air temperature of 7°C), the compressor speed must also increase in order to keep satisfying the heating demand. Therefore, the higher the desired water temperature, the louder the heat pump operation will be.

At the quantitative example of Figure 29, one can observe that the evolution of the load of a heat pump is likely to feature a direct correlation to its radiated sound power level. Such load can evolve over time, with variations of external parameters such as the temperature gap to the target (this example) or with domestic hot water (DHW) tapping.

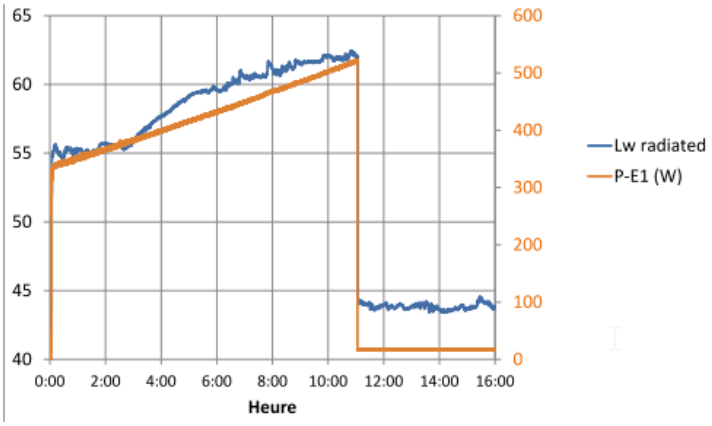


**Figure 29: Time evolution of the radiated SWL vs electrical consumption of a thermodynamic water boiler as the water temperature closes in on the target temperature (indicator of the load). Extract of internal Annex measurements.**

The following example from DTI's internal measurements (see Table below and Figure 30) shows an increase of 3dB of the sound power level in connection with an increase of the supply water temperature from 35°C to 55°C, for almost the same heating capacity.

| | | A7/W35 | A7/W55 |
|---|---|---|---|
| Heating capacity | kW | 7.0 | 7.3 |
| COP | - | 4.4 | 2.9 |
| Power input | kW | 1.6 | 2.5 |
| Outdoor heat exchanger inlet | °C | 7.0 | 7.0 |
| Outdoor heat exchanger outlet | °C | - | - |
| Indoor heat exchanger inlet | °C | 30.0 | 47.0 |
| Indoor heat exchanger outlet | °C | 35.0 | 55.0 |
| Compressor speed | Hz | 51 | 57 |
| Fan speed | rpm | 580 | 620 |
| Sound power level | dB(A) | 59.0 | 62.0 |

The load increases and the compressor and fan speeds slightly increase in order to maintain the heating demand when supplying a water temperature of 55°C, while the COP sinks significantly.

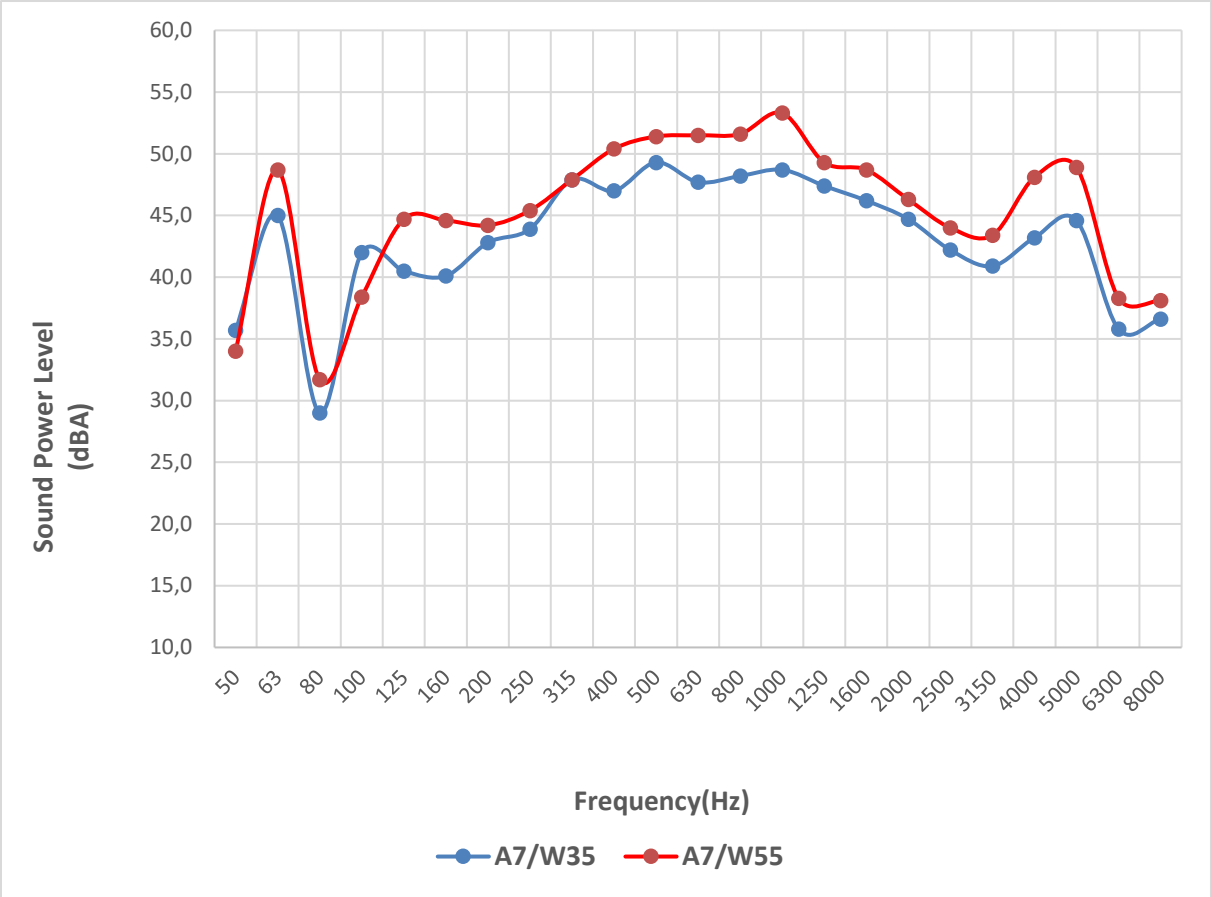


**Figure 30: Sound characteristics of an air-to-water heat pump at the typical A7/W35 and A7/W55 operating conditions. The total $L_{WA}$ increases of 3.0dB from A7/W35 to A7/W55. (source DTI)**

## Different operation conditions and related control strategies

Depending of the heat pump type, the following operation conditions can occur:

- Full load (stationary energetic state)
- Part load (stationary energetic state)
- Silent mode (control strategy inducing operation at lower capacity with specific speeds)
- Defrosting mode (necessary transient operation of air-to-water devices)

A change of operating condition can cause a significant change in the noise character, while the overall noise level additionally depends on the type of heat pump and its construction.

The following example from DTI's internal measurements (see Table below and Figure 31) illustrates the difference between full load condition and silent mode condition for the same temperature condition of A7/W55 for an air to water heat pump.

| | | A7/W55_silent mode | A7/W55 |
|---|---|---|---|
| Heating capacity | kW | 5.4 | 7.3 |
| COP | - | 3.0 | 2.9 |
| Power input | kW | 1.8 | 2.5 |
| Outdoor heat exchanger inlet | °C | 7.0 | 7.0 |
| Outdoor heat exchanger outlet | °C | - | - |
| Indoor heat exchanger inlet | °C | 47.0 | 47.0 |
| Indoor heat exchanger outlet | °C | 55.0 | 55.0 |
| Compressor speed | Hz | 43 | 57 |
| Fan speed | rpm | 470 | 620 |
| Sound power level | dB(A) | 57.0 | 62.0 |

It is worth noting that the COP is almost the same for both modes. For the silent mode, the sound power lever is reduced by 5 dB, but due to a reduction in the compressor speed and the fan speed, the heating capacity is reduced by 26 % as well.

The relevance of such operation mode comes with control strategy: a model-based control approach with simplified models can be used to calculate a maximum night reduction of the compressor speed. In other words, if the compressor is the loudest component, the heat pump demand for heating/cooling energy can be divided during part load operation for one day in such a way that the heat pump runs at full load during the day and operates in silent mode at a lower thermal output and thus at low compressor speed or sound power overnight.

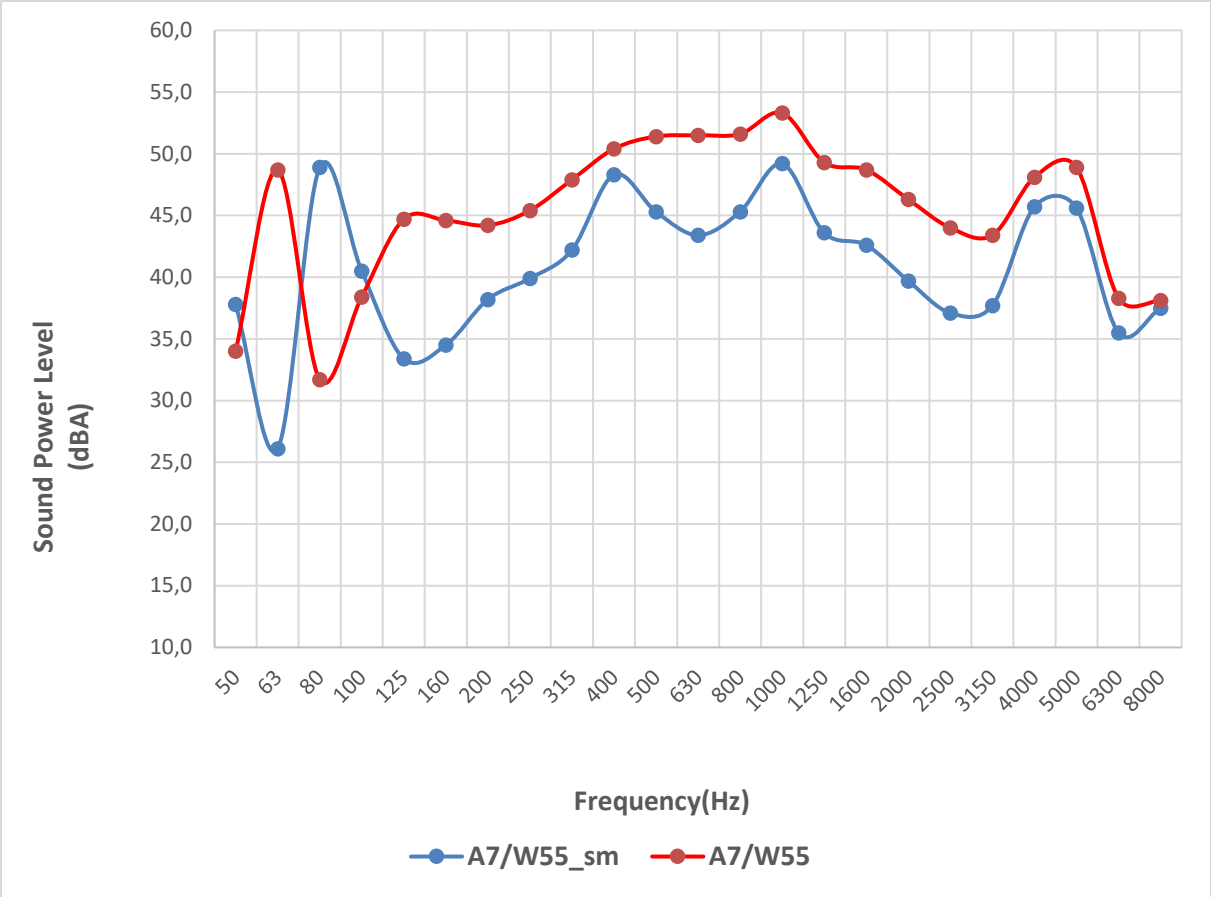


**Figure 31: Sound characteristics of an air-to-water heat pump for A7/W55 in silent mode versus normal A7/W55 operation. (source DTI)**

How far the speed can be reduced depends on a number of external parameters such as outside temperature, heating/cooling load, etc.

Experiments at AIT showed that fewer on / off switching operations at A2W35, along with shorter operating times at night and partial load operation during the night lead to a 10dB(A) nightly reduction (12h) for a daytime increase of only 4.5dB(A) (partial load all day with 69 dB(A) or night: 58.8 dB(A) and day 73.5 dB(A) ).

With such an efficient noise diminution with such easy implementation, load shifting and "Silent Modes" are now common procedures for modern heat pumps.

# Conclusion

It has first been reported about the main software possibilities to model the acoustic impact of heat pump operating conditions (some of which could be implemented within the heat pump real time control strategy). Then the physical processes at the origin of those noise variations and their acoustic signatures have been described and exemplified.

For heat pump operation, transient noises are found to be quieter than steady noises near full capacity, but remain very relevant in the effort to improve the acoustics of heat pumps, as they tend to draw more attention through their suddenness or evolutive character (+ strong tonality for some).

Amongst the means to reduce their impact, one can distinguish two categories:

- The same usual measures as for steady state noises (isolation and damping for components and housing, construction of adapted components)
- Strategies of control to reduce their amplitude or frequency of occurrence (operation level adapted to load to avoid modulation, delays, triggers, time of day)

# References


[1] 2018. Energy Atlas. *Facts and figures about renewables in Europe* https://www.boell.de/en/energy-atlas-figures-and-facts-about-renewables-europe.

[2] J. Emhofer, R. Zitzenbacher, and C. Reichl. 2017. Sound Source Extension Library for Modelica. In . Linköping Electronic Conference Proceedings. Linköping University Electronic Press, 605–612. DOI: https://doi.org/10.3384/ecp17132605.

[3] Karlheinz Bay, Jens Röhlfing, Sebastian Wagner, Thore Oltersdorf, Thomas Gindre, Lena Schnabel, Hannes Fugmann, Omar Abu-Khass. Wärmepumpen - Akustik und Mehrquellensysteme. BMWi FKZ 03ET1535A.

[4] Müller D., Lauster M., Constantin A., Fuchs M., Remmen P. 2016. AixLib - An Open-Source Modelica Library within the IEA-EBC Annex 60 Framework. *BauSIM*, 3–9.

[5] C. Vering et al. 2018. Transiente Modellierung eines Verdichters zum Vergleich von niedrig GWP Kältemitteln für Kompressionswärmepumpen. *BauSIM*.

[6] M. Popovac, J. Emhofer, E. Wasinger, P. Wimberger, R. Zitzenbacher, D. Meisl, F. Linhardt, N. Schmiedbauer, Ch. Reichl. 2018. OpenFOAM implementation of algebraic frosting model and its application on heat pump evaporators. In *Gustav Lorentzen Conference 2018*. IIR, Paris.

[7] Christoph Reichl, Andreas Strehlow, Thore Oltersdorf, Simon Braungardt, Marco Pröhl, Peter Benovsky, Mirza Popovac, Thomas Fleckl. 2015. GreenHP: Next Generation Heat Pump for Retrofitting Buildings - New Evaporator Component for Large Capacity Air-to-Water Heat Pumps. In *REHVA Annual Conference 2015 "Advanced HVAC and Natural Gas Technologies"*. Annual Conference, Brussels, 100–109.

[8] C. Reichl, J. Emhofer, P. Wimberger, N. Schmiedbauer, F. Linhardt, E. Wasinger, C. Köfinger, and T. Fleckl. SilentAirHP - Analyse und Entwicklung von Schallreduktionsverfahren fuer Luft-Wasser-Wärmepumpen.

[9] Nikolai Kleinfeller, Joachim Bös, and Tobias Melz. 2019. Measurement of the structural intensity of curved shell structures by means of 3D laser vibrometry. *DAGA Annual Conference*.

[10] Thorsten Stöwer. 2018. Berechnung der Strukturintensität von Fahrzeugstrukturen. PhD. Institute of System Reliability, Adaptive Structures and Machine Acoustics. Technical University, Darmstadt.

[11] F. Linhardt, K. Alten, J. Emhofer, C. Köfinger, T. Fleckl, P. Wimberger, M. Gröschl, and C. Reichl. 2017. Charakterisierung der Schallabstrahlung von Luft-Wasser-Wärmepumpen mittels simultaner Hitzdrahtanemometrie, Vibrationsmessung und Schalldruckbestimmung. *DAGA Annual Conference*.

[12] S. Derr and C. Burkhart. 2015. Schallabstrahlung von Luftwärmepumpen. *DAGA Annual Conference*.

[13] C. Neuhaus, A. Lion, M. Johlitz, P. Heuler, M. Barkhoff, and F. Duisen. 2017. Fatigue behaviour of an elastomer under consideration of ageing effects. *International Journal of Fatigue* 104, 72–80. DOI: https://doi.org/10.1016/j.ijfatigue.2017.07.010.

[14] S. Kluth, C. Schulze, J. Hübelt, M. Ruhnau, S. Richardt, R. Krause, A. Peusch, C. Fabris. 2014. Ermittlung der Geräuschemission und Möglichkeiten zur Lärmminderung bei Luft-Wasser-Wärmepumpen. *DAGA Annual Conference*.

[15] O. Gustafsson, C. Teuillieres, H. Hellgren, M. Axell, and J.-O. Dalenbäck. 2016. Reversing air-source heat pumps – Noise at defrost initiation and a noise reducing strategy. *International Journal of Refrigeration* 62, 137–144. DOI: https://doi.org/10.1016/j.ijrefrig.2015.10.017.

www.heatpumpingtechnologies.org

**Heat Pump Centre**
c/o RISE - Research Institutes of Sweden
PO Box 857
SE-501 15 BORÅS
Sweden
Tel: +46 10 516 5512
E-mail: hpc@heatpumpcentre.org

**www.heatpumpingtechnologies.org**

Report no. HPT-AN51-10